

國立交通大學

電子工程學系 電子研究所碩士班

碩 士 論 文

可相容高工作電壓且具有負載適應性之抑制癲癇

發作電流刺激器設計

**Design of High-Voltage-Tolerant Stimulus Driver to
Suppress Epileptic Seizure with Adaptive Loading**

Consideration in Low-Voltage Process

研 究 生：李易儒 (Yi-Ju Li)

指 導 教 授：柯明道教授 (Prof. Ming-Dou Ker)

中華民國一百年七月

可相容高工作電壓且具有負載適應性之抑制癲癇
發作電流刺激器設計

**Design of High-Voltage-Tolerant Stimulus Driver to
Suppress Epileptic Seizure with Adaptive Loading
Consideration in Low-Voltage Process**

研究生：李易儒

Student: Yi-Ju Li

指導教授：柯明道教授

Advisor: Prof. Ming-Dou Ker



A Thesis

Submitted to Department of Electronics Engineering and Institute of
Electronics College of Electrical and Computer Engineering

National Chiao-Tung University

in Partial Fulfillment of the Requirements

for the Degree of

Master

in

Electronics Engineering

July 2011

Hsin-Chu, Taiwan

中華民國一百年七月

可相容高工作電壓且具有負載適應性之抑制癲癇 發作電流刺激器設計

學生：李 易 儒

指導教授：柯 明 道 教授

國立交通大學

電子工程學系 電子研究所碩士班

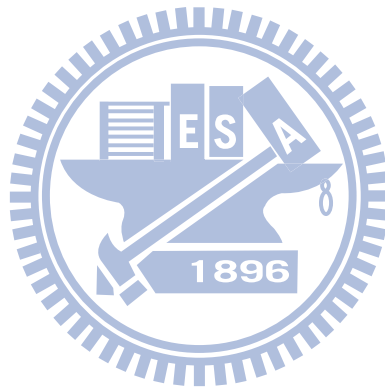


Abstract (Chinese)

電刺激技術已是一種常見的醫療方式，例如功能性電刺激 (functional electrical stimulation, FET) 與治療性電刺激 (therapeutic electrical stimulation, TES)。透過電流訊號流過患者的待刺激部位，可使患者恢復部分身體的機能。而隨著積體電路製程的微縮化，整合智慧型仿生系統於單晶片的目標已變得可行，此系統單晶片可植入動物體，以對患部進行電刺激。對植入性晶片而言，設計時的主要考量為安全性、可靠度與功率消耗。

本文所提出的電路為可相容高工作電壓且具有負載適應性之抑制癲癇發作電

流刺激器。由於在刺激器輸出刺激電流時，輸出端會有將近十伏特的高壓產生，為了承受輸出端的高壓，過去的刺激器電路都是使用高壓製程來實作，而本刺激器電路為了與智慧型仿生系統中的其他電路做單晶片整合，因此必須使用低壓製程來實作。本刺激器透過電路設計的技巧，使其能以低壓製程元件來承受高壓，而電晶體不會面臨電性過壓的情形。此外，當待刺激部位的阻抗在設計的範圍內變化時，電流刺激器亦能提供穩定的刺激電流。最後，本設計已由動物實驗獲得驗證，刺激器可有效地抑制老鼠的癲癇病症發作。



Design of High-Voltage-Tolerant Stimulus Driver to Suppress Epileptic Seizure with Adaptive Loading Consideration in Low-Voltage CMOS Process

Student: Yi-Ju Li

Advisor: Prof. Ming-Dou Ker

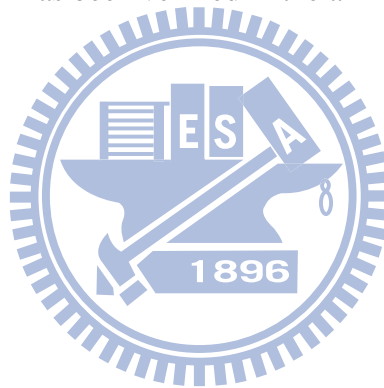
*Department of Electronics Engineering & Institute of Electronics
National Chiao-Tung University*



The treatment of using a stimulus driver has been investigated and verified. By stimulating the nerves may recover the patient's physical functions. It can be applied to functional electrical stimulation and therapeutic electrical stimulation. As the CMOS process developed, using an implantable device to provide stimulus current can be accomplished. The main considerations of designing an implantable device are safety, reliability, and power consumption.

The proposed stimulus driver is utilized to suppress epileptic seizure. Due to the

loading impedance is hundreds $k\Omega$ and the stimulus current is tens μA , the voltage at the output of stimulus driver is ~ 10 V. Conventional works are fabricated in high-voltage process in order to sustain the high voltage at output of stimulus driver. To be integrated with other circuits into SoC, this work is implemented in low-voltage process. By designing the structure, this work fabricated in $0.18\text{-}\mu m$ $1.8\text{-}V/3.3\text{-}V$ CMOS process is able to sustain high voltage (~ 10 V) without gate-oxide overstress. It can provide stimulus current ~ 40 μA as the loading impedance varies from 100 $k\Omega$ to 250 $k\Omega$. The function of this work has been verified in the animal test experiment.



Acknowledgment

在這兩年中，很感謝柯明道老師的指導，讓我學到了很多東西，特別是當我還沒確定研究的題目時，老師給了我研究的方向，除了在課業與研究方面之外，老師的話常常會帶給我們很多啟發，讓我們學到許多人生中的道理。

感謝實驗室的學長姐們，借我 ISSCC 的正哥、cover 整個碩班的小胖學長、小王學長、陳穩義學長、剛升格當爸的葉致廷學長、帶給我們歡樂的小州哥、竹立煒學長、蔡惠雯學姐、林倍如學姐，還有去年從碩班畢業的林佑達、陳韋霖、張堂龍、今年跟我們一起畢業的陳思翰。除了會給我一些研究上的建議之外，平常 meeting 時大家一起討論各種大小事務，讓我的研究生涯更充實。特別要感謝的是林群祐學長，從去年開始接癲癇刺激器的計畫之後，各種大大小小的問題他都能幫我解決，我想如果沒有他的幫忙，我大概無法如期畢業吧！

還有同屆跟我一起做研究的三位夥伴，黃筱晴、林宛彥、艾飛，雖然他們都是做 ESD 相關的研究，跟我的研究方向不同，但若碰到 ESD 或元件相關的問題，就能找他們一起討論，而跟艾飛聊天的過程中，讓我發現我的英文真的有待加強...，這兩年有大家的陪伴，讓我覺得求學路上並不孤單，也為我的生活增添許多色彩。

另外還要感謝成大資工所的阿成，沒有他，我就沒辦法完成我的動物實驗，雖然他自己事情也很多，但每次我向他求助的時候，他都很熱心地幫助我。

最後還要感謝我的家人與朋友們，和你們大家互吐苦水、分享生活點滴，都是讓我繼續往前的動力，真的謝謝你們！

李易儒

Contents

Abstract (Chinese)	i
Abstract (English)	iii
Acknowledgment	v
Contents	vi
Table Captions	viii
Figure Captions	ix
Chapter 1 Introduction	1
1.1 Motivation	1
1.2 Thesis Organization	3
Chapter 2 Background of Epilepsy, Effective Treatments for Epilepsy, Epileptic Seizure Detecting and Controlling System, and Design of Implantable Stimulus Driver	4
2.1 Overview of Epilepsy	4
2.2 Effective Treatments for Epilepsy	8
2.2.1 Available Epilepsy Treatment	8
2.2.2 Epileptic Seizure Detecting and Controlling System	11
2.3 Brief Introduction of Implantable Stimulus Driver Technique	12
Chapter 3 Design of High-Voltage-Tolerant Stimulus Driver to Suppress Epileptic Seizure with Adaptive Loading Consideration in 0.18-μm CMOS Process	17
3.1 Introduction	17
3.2 Novel High-Voltage-Tolerant Stimulus Driver with Adaptive Loading Consideration Fabricated in 0.18- μ m CMOS Process	19
3.2.1 Implementation	19
3.2.2 Simulation Results	31
3.2.3 Measurement Results	37
3.2.4 Integration of the Proposed Stimulus Driver and Epileptic Seizure	

<i>Monitoring and Controlling System</i>	44
3.3 Summary	48
Chapter 4 Conclusions and Future Works	49
4.1 Conclusions	49
4.2 Future Works	51
4.2.1 Integration with Charge Pump System	51
4.2.2 An Additional Slew-rate Clamping Circuit Should Be Added	52
4.2.3 Design of Bi-Phase Stimulus Driver	53
References	56
Vita	60

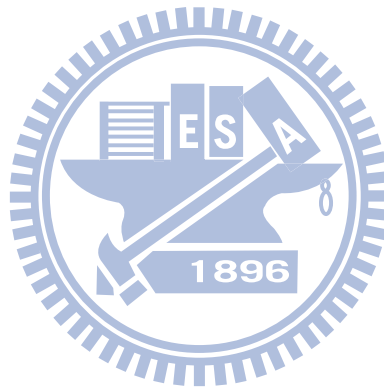


Table Captions

Table 3.1. Relationship of V_1 , V_2 , comparator outputs, control signals, operating voltage, and reference voltage.	27
Table 4.1. Summary of the proposed stimulus driver.	50

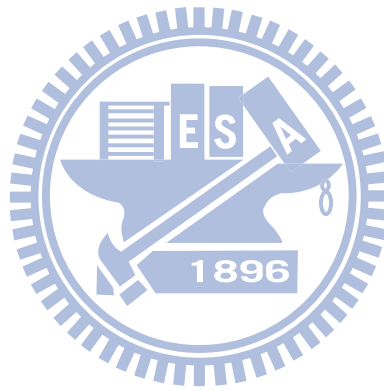


Figure Captions

Fig. 2.1.	Nervous system in the human body [9].	5
Fig. 2.2.	The way neurons transmit signals is that (a) ions are transferred through membrane and accumulate at synapse to generate (b) action potential [10].	5
Fig. 2.3.	Brain activities under different states [11], [12].	7
Fig. 2.4.	Left side picture is an electrode array that is used to record long-term brain activities of a patient. Right side picture is EEG of an epileptic patient, channels with black mark indicates that epileptic seizure occurs, channel with gray mark indicates nearby area that is affected by abnormal discharge which forms epileptic seizure [13].	7
Fig. 2.5.	Vagus nerve stimulation [18].	10
Fig. 2.6.	Deep brain stimulation [20].	10
Fig. 2.7.	The closed-loop epileptic seizure monitor and controller system consisted of (a) microcontroller board, (b) signal conditioning board, and (c) stimulator board [28].	12
Fig. 2.8.	Stimulator output stage with blocking capacitor [30].	15
Fig. 2.9.	Wide swing cascade current source of stimulator [33].	15
Fig. 2.10.	Voltage controlled resistor current source of stimulator [34].	16
Fig. 3.1.	The block diagram of an implantable stimulus driver for epilepsy treatment.	18
Fig. 3.2.	Block diagram of the proposed stimulus driver.	19
Fig. 3.3.	Structure of output driver fabricated in 0.18- μm 1.8-V/3.3-V CMOS process. 3.3-V transistors are shown with thick gate oxide, and 1.8-V transistors are shown with thin gate oxide.	20
Fig. 3.4.	Voltage conditions of each node in output driver circuit as operating voltage $V_{cc} = 5.04$ V.	22
Fig. 3.5.	Voltage conditions of each node in output driver circuit as operating voltage $V_{cc} = 6.48$ V.	22
Fig. 3.6.	Voltage conditions of each node in output driver circuit as operating voltage $V_{cc} = 7.92$ V.	23
Fig. 3.7.	Voltage conditions of each node in output driver circuit as operating voltage $V_{cc} = 9.36$ V.	23
Fig. 3.8.	The V_{cc} control circuit consisted of three comparators and logic gates.	24
Fig. 3.9.	Structure of comparator in V_{cc} control circuit.	25

Fig. 3.10.	K-map of control signals A and B derived from Table 3.1.	27
Fig. 3.11.	The related logic gates of Eq. (3-1) and (3-2).	28
Fig. 3.12.	The charge pump system.	29
Fig. 3.13	Reference voltage selector in the charge pump system. With selected $r_1 \sim r_5$, the value of V_{ref} depends on control signals A/B.	29
Fig. 3.14.	Operating voltage of conventional design and that of proposed stimulus driver verses tissue impedance.	31
Fig. 3.15.	The simulation results of stimulus current and control signals as loading impedance $R_L = 250 \text{ k}\Omega$ and operating voltage $V_{cc} = 5.04 \text{ V}$.	32
Fig. 3.16.	The simulation results of stimulus current and control signals as loading impedance $R_L = 250 \text{ k}\Omega$ and operating voltage $V_{cc} = 6.48 \text{ V}$.	33
Fig. 3.17.	The simulation results of stimulus current and control signals as loading impedance $R_L = 250 \text{ k}\Omega$ and operating voltage $V_{cc} = 7.92 \text{ V}$.	33
Fig. 3.18.	The simulation results of stimulus current and control signals as loading impedance $R_L = 250 \text{ k}\Omega$ and operating voltage $V_{cc} = 9.36 \text{ V}$.	34
Fig. 3.19.	Simulation results of stimulus current as loading impedance $R_L = 100 \text{ k}\Omega$ and $250 \text{ k}\Omega$ with their corresponding V_{cc} .	34
Fig. 3.20.	Simulation results of stimulus current as loading impedance varying from $100 \text{ k}\Omega$ to $250 \text{ k}\Omega$.	35
Fig. 3.21.	Simulation results of operating voltage as loading impedance varying from $100 \text{ k}\Omega$ to $250 \text{ k}\Omega$.	36
Fig. 3.22.	Simulation results of power consumption as loading impedance varying from $100 \text{ k}\Omega$ to $250 \text{ k}\Omega$.	36
Fig. 3.23.	(a) Layout and (b) chip photo of the proposed stimulus driver.	37
Fig. 3.24.	Measurement setup of this work. Two Keithley 2400 source meters are used to provide system supply voltage (V_{DD}) and operating voltage (V_{cc}). HP 33120A function generator is utilized to provide the stimulation signal (V_{ST}). TDS 3054B is used to observe output voltage of the stimulus driver and control signals A and B.	38
Fig. 3.25.	The measurement results of stimulus current and control signals as loading impedance $R_L = 250 \text{ k}\Omega$ and operating voltage $V_{cc} = 5.04 \text{ V}$.	39
Fig. 3.26.	The measurement results of stimulus current and control signals as loading impedance $R_L = 250 \text{ k}\Omega$ and operating voltage $V_{cc} = 6.48 \text{ V}$.	40
Fig. 3.27.	The measurement results of stimulus current and control signals as loading impedance $R_L = 250 \text{ k}\Omega$ and operating voltage $V_{cc} = 7.92 \text{ V}$.	40

Fig. 3.28.	The measurement results of stimulus current and control signals as loading impedance $R_L = 250 \text{ k}\Omega$ and operating voltage $V_{cc} = 9.36 \text{ V}$.	41
Fig. 3.29.	Measurement results of stimulus current as loading impedance $R_L = 100 \text{ k}\Omega$ and $250 \text{ k}\Omega$ with their corresponding V_{cc} .	41
Fig. 3.30.	Measurement results of stimulus current as loading impedance varying from $100 \text{ k}\Omega$ to $250 \text{ k}\Omega$.	42
Fig. 3.31.	Measurement results of operating voltage as loading impedance varying from $100 \text{ k}\Omega$ to $250 \text{ k}\Omega$.	43
Fig. 3.32.	Measurement results of power consumption as loading impedance varying from $100 \text{ k}\Omega$ to $250 \text{ k}\Omega$.	43
Fig. 3.33.	Measurement setup of integration experiment of proposed stimulus driver and closed-loop epileptic seizure monitoring and controlling system. (a) Long-evans rats in this experiment, and (b) the proposed stimulus driver.	45
Fig. 3.34.	The closed-loop epileptic seizure monitoring and controlling system utilized in this animal test experiment.	45
Fig. 3.35.	The waveform of stimulus current provided by the proposed stimulus driver in this animal test experiment.	46
Fig. 3.36.	The EEG of the Long-Evans rat under (a) normal condition and (b) epileptic seizure in this animal test experiment.	47
Fig. 3.37.	The procedure of normal condition, epileptic seizure, stimulus driver activated, and epileptic seizure suppressed.	47
Fig. 4.1.	Stimulus driver integrated with charge pump system.	51
Fig. 4.2.	The waveform of voltage observed at the electrode while stimulating the rat's brain tissue with fixed stimulus current of $20 \text{ }\mu\text{A}$ (800 Hz , duty cycle = 40%).	52
Fig. 4.3.	The waveform of voltage drop across a resistor ($200 \text{ k}\Omega$) while stimulus current of $20 \text{ }\mu\text{A}$ (800 Hz , duty cycle = 40%) flowing through it.	53
Fig. 4.4.	Bi-phase stimulus driver with both positive and negative powers provides biphasic stimulus current through one electrode per stimulus site.	54
Fig. 4.5.	Bi-phase stimulus driver with only positive power provides biphasic current between two electrodes per stimulus site.	54
Fig. 4.6.	The method to implement biphasic stimulus current by making a copy of the output driver and placing it symmetrically to the origin circuit.	55

Chapter 1

Introduction

1.1 Motivation

As medical science and electronics engineering developed, new technologies combining medicine and microelectronics technology have been investigated and demonstrated. The applications of bioelectronics lead to a new generation of healthcare and therapies. There are several fabulous applications of bioelectronics such as magnetic resonance imaging and electroencephalography (EEG) that cause a revolution in medical science. In recent decades, it has been demonstrated that functional electrical stimulation (FES) and therapeutic electrical stimulation (TES) that transmit artificial electrical signals into nervous system can restore some physical functions of a human [1]. Hence the relationship between electrical transaction and nervous system has become indivisible. FES and TES have been studied for innovative medical treatments in different applications such as cardiac pacing, muscle exercising and even vision restoration [2]. Epilepsy is also one of diseases investigated to be treated by therapeutic electrical stimulation.

Epilepsy is the second most common neurological diseases, which is caused by transient abnormal discharge activity in brain. The incidence rates of epileptic seizures were found to be 1 % [3], which means there are tens of millions of people who suffer from epilepsy in the world. As medical science developed, some traditional therapies to cure epileptic seizure have been proposed such as pharmacologic treatment and surgical treatment. For a patient who suffers from epilepsy, pharmacologic treatment is the most

common used in the first place. However, some patients do not respond to the medicament, and there may be heavy side effects while taking pharmacologic treatment. For those conditions mentioned above, the surgical treatment is in common use. The non-reversible brain surgery is risky that might cause permanent functional losses. In addition, only 75% of patients do response well to the traditional therapies. Nowadays, epilepsy becomes predictable by analyzing EEG in time or frequency domains [4]. Several ways to predict epileptic seizure have been researched such as predictable features and prediction by classification. It has also been demonstrated that the abnormal discharge signal that causes epileptic seizure can be suppressed by TES before epilepsy happens [5]. To be compared with the non-reversible surgical treatment, the advantages of electrical stimulation treatment are flexible, recoverable, and non-destructive. It is more harmless to tissue in brain.

Though, TES is a feasible way to suppress epileptic seizure or cure other diseases, there are still several problems needed to be solved while providing the stimulus current for TES. Due to different kinds of tissue, locations, and implanted time, the equivalent impedance of electrode and tissue will vary in a wide range. The tissue impedance for individuals ranges from tens $k\Omega$ to hundreds $k\Omega$. To provide fixed magnitude of stimulus current, the output voltage varies in a wide range corresponding to the tissue impedance. In addition, high operating voltage may result in problems of gate-oxide overstress, hot-carrier effect, and other reliability issues [6], [7], [8]. Furthermore, to an implantable device, power consumption is also an important consideration because it is inversely proportional to the use time. In this thesis, the proposed stimulus driver takes both reliability and power consumption into consideration. The stimulus driver with high-voltage-tolerant structure and the method of regulation of operating voltage to reduce power consumption are investigated and verified in this work.

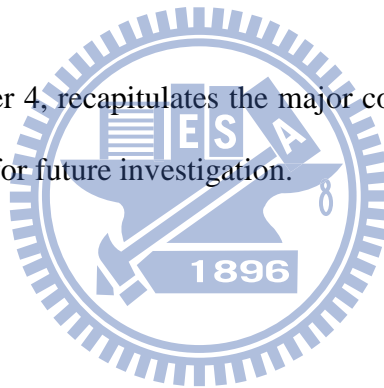
1.2 Thesis Organization

The first chapter, chapter 1, includes the motivation of this work and the thesis organization.

The chapter 2 of this thesis introduces some background knowledge of epilepsy, epileptic seizure treatments, and design of implantable stimulus driver.

In the chapter 3, a new design of high-voltage-tolerant stimulus driver to suppress epileptic seizure with adaptive loading consideration is proposed. The integration of the proposed stimulus driver and closed-loop epileptic seizure monitoring and controlling system has been implemented and the function has been verified in the animal test experiment.

The last chapter, chapter 4, recapitulates the major consideration of this thesis and concludes with suggestions for future investigation.



Chapter 2

Background of Epilepsy, Effective Treatments for Epilepsy, Epileptic Seizure Detecting and Controlling System, and Design of Implantable Stimulus Driver

2.1 Overview of Epilepsy

Epilepsy, the second most common neurological disease in the world, is caused by abnormal discharge of cells in brain. Brain to a human body is like a central process unit to a computer. It controls not only almost all the actions of a human but also sensations, emotions, memories, and so on. Signals between brain and different parts of body are delivered through the nervous system which consists of hundreds of thousands of neurons. Fig. 2.1 shows the nervous system in a human body which covers from head to toe [9]. Signals of actions from brain to organs are delivered by motor neurons, and signals of sensations from organs to brain are transmitted through sensory neurons. The way to pass a signal from one neuron to another is to excite it by chemical or electrical stimulation [10]. When a signal is going to be transmitted to the next neuron, some ions such as sodium, potassium, and chlorine are transferred through the ion channel to accumulate at the synapse as shown in Fig. 2.2(a). Accumulated ions cause the change of concentration of ions and voltage gradient of the membrane of neurons. If the voltage gradient exceeds the action potential to excite the neuron as shown in Fig. 2.2(b), the neuron will be triggered and the signal can be transmitted from the present neuron to the

next one. By a chain of this kind of electrical stimulations, signals can be transmitted between brain and different parts of human body.

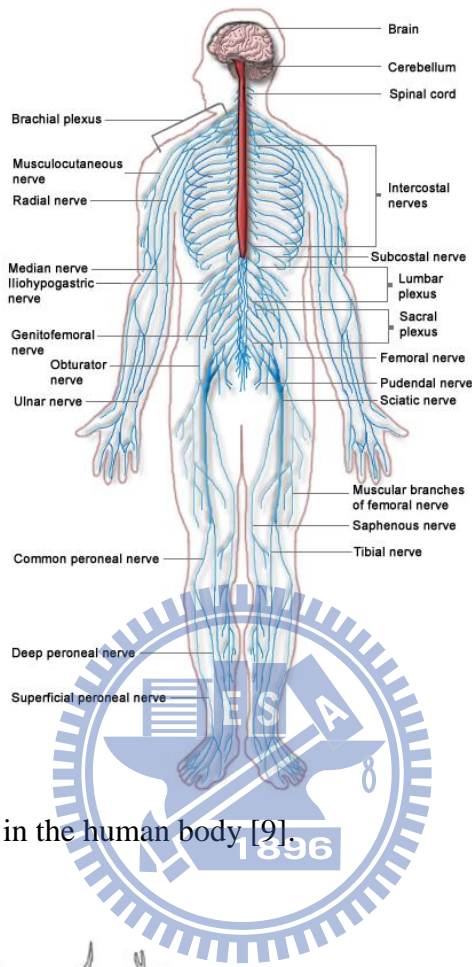


Fig. 2.1. Nervous system in the human body [9].

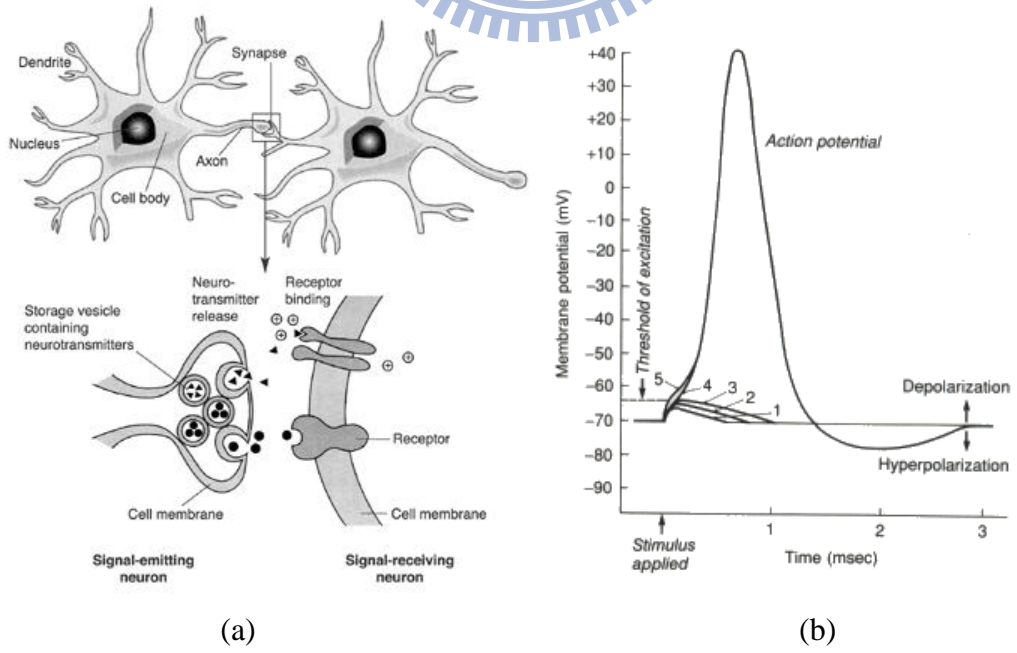


Fig. 2.2. The way neurons transmit signals is that (a) ions are transferred through membrane and accumulate at synapse to generate (b) action potential [10].

Under normal brain activity, brain generates constant and stable electrical signals in certain patterns. Fig. 2.3 shows different waveforms of EEG depending on states of body under normal conditions [11], [12]. These signals transmit along neurons of nervous system in the brain, spinal cord, and ganglia to whole body via neurotransmitters. During epileptic seizure time, abnormal discharges flow through nearby neurons and tissues. Like flowing through a resistor, current flows through nearby tissues will cause voltage drop. If the voltage exceeds the action potential, neurons will be triggered and unexpected signals will be spread out. In this case, normal activities of brain may be interrupted, and patients' normal physical and emotional functions may be affected. Right side picture of Fig. 2.4 shows the EEG under abnormal brain activities recorded by the electrode array [13].

Due to the intensity of seizure, epilepsy can be roughly classified into two types: one is partial seizure, and the other is generalized seizure [14]. Partial seizure, which means abnormal discharge occurs just on one location of the brain, includes simple partial seizure and complex partial seizure. The difference between them is whether patients keep on conscious or unconscious during epileptic seizure time. When simple partial seizure occurs, patients remain conscious and can remember what happened during the seizure period. But, emotions, sensations, and motions are affected. Complex partial seizure has a greater influence on patients. During the seizure time, patients can not behave normally, control their motions, talk with other people, and so on. It is because patients usually become unconscious during complex partial seizure period, they won't remember what happened after epileptic seizure.

According to different causes, syndromes, and locations of seizures, epilepsy can be classified into more than 40 types. Each type of epilepsy has unique seizure form, age group of patients, diagnosis, and treatment. Although most types of epileptic seizure won't last a long time which may prolong only one or two minutes, epilepsy still affects

patients' daily life deeply. Effective treatments to cure all the patients should be investigated.

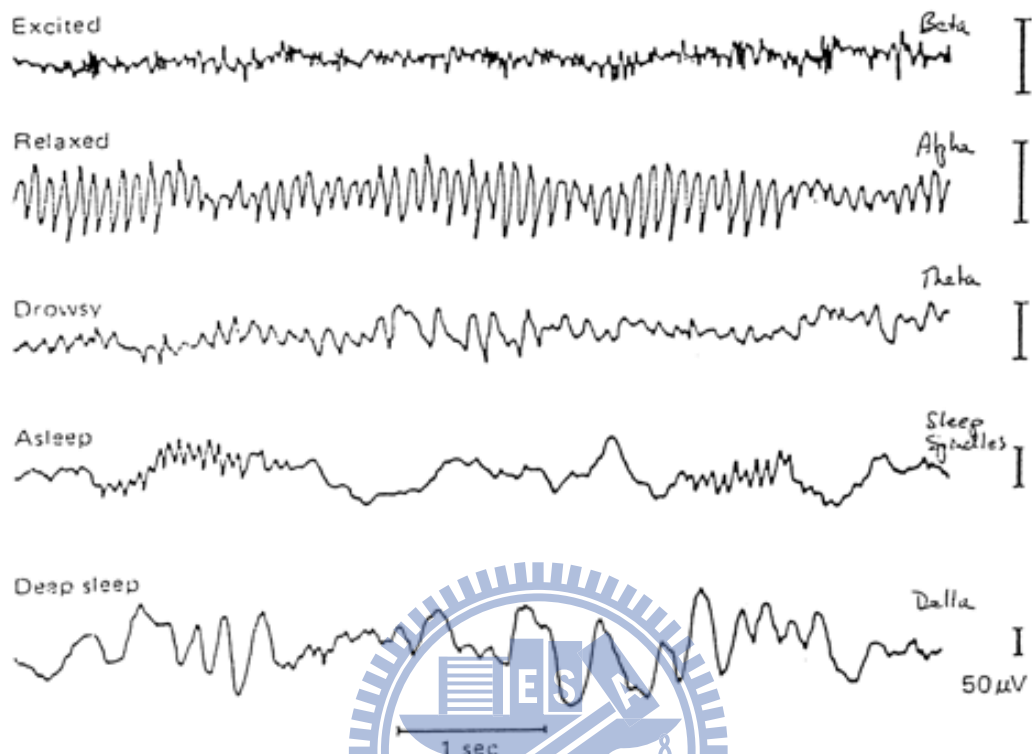


Fig. 2.3. Brain activities under different states [11], [12].

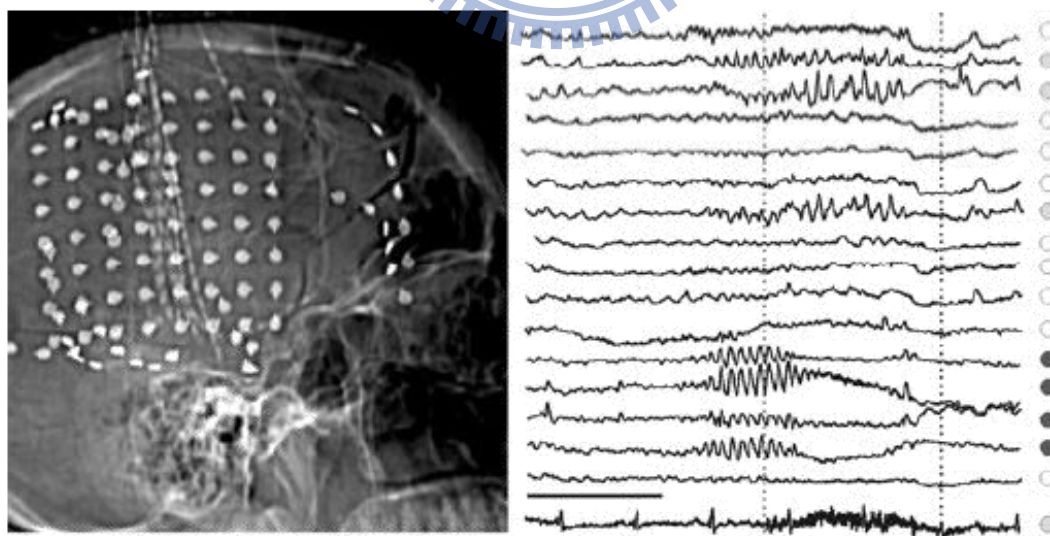


Fig. 2.4. Left side picture is an electrode array that is used to record long-term brain activities of a patient. Right side picture is EEG of an epileptic patient, channels with black mark indicates that epileptic seizure occurs, channel with gray mark indicates nearby area that is affected by abnormal discharge which forms epileptic seizure [13].

2.2 Effective Treatments for Epilepsy

2.2.1 Available Epilepsy Treatment

Pharmacologic treatment is the most common way used to suppress epileptic seizure. Due to the diversification of epilepsy, there are more than 20 types of medications, and each is developed for specific type of epileptic seizure. According to patients' age, types of epilepsy, syndromes, and intensity of seizure, doctors will choose suitable medications (antiepileptic drugs or AED) for treatment. There are two types of AEDs which can be used: one is narrow spectrum AEDs, and the other is broad spectrum AEDs. While the narrow spectrum AEDs focus on small number of epileptic seizure, the broad spectrum AEDs work for a large group of seizure. However, epilepsy is a complicated disease. There is no standard recipe to decide which medication is the best for an epileptic patient. Besides the effectiveness, side effects are also the mainly consideration for a doctor to write out a prescription. Most of patients' condition of seizure can be ameliorated by AEDs. However, every kind of medicines might sometimes lead to side effects including blurry vision, dizziness, headaches, and fatigue [15]. In addition, these medications might lead to allergic in roughly 10 % of people and can impair blood cell or liver. Unfortunately, there are still many patients who do not respond to AEDs, which is called medically refractory. For these patients, other treatments should be taken into consideration such as surgical treatment.

Surgical treatment is an alternative for those medically refractory patients whose epileptic seizure cannot be controlled by medications [16]. Before the surgery, a cautious evaluation of the patient is taken. Through the evaluation, the brain location that abnormally discharges is located. Besides the brain areas, the functions which may be affected are found out as well. The evaluation includes long-term EEG recording, neurological examination, MRI, and so on. What kind of surgery is applied depends on

different kind of seizure and the location of the brain. There are two basic brain surgeries for epilepsy: one is resection surgery, and the other is disconnection surgery. In the resection surgery, the surgeon removes abnormal brain areas that initiate seizure. The most common type of resection surgery is temporal lobectomy. In disconnection surgery, which is sometimes called functional disconnection, the surgeon interrupts the nerve directions that spread abnormal discharges. Surgical treatment is not a suitable option for every patient whose seizure cannot be ameliorated by medications. Because some sections of brain are too important to be removed by the surgery. It is a risky treatment because patients may lose some physical functions permanently after taking the surgery. In addition, there is no guarantee that epileptic seizure can be cured completely by surgery.

Expect for traditional treatments such as pharmacologic treatment and surgical treatment mentioned above, electrical stimulation is an innovative treatment for drug-resistant epilepsy [17]. It has been investigated and approved currently. Advantages of electrical stimulation are flexible, recoverable, and non-destructive. Vagus nerve stimulation (VNS), is one kind of electrical treatment [18], [19]. The vagus nerve is autonomic nervous system, which controls physical functions that are not under voluntary control. The vagus nerve is situated the neck and connects abdomen and the lower part of brain. Device of VNS consists of pulse generator, flexible wires, and electrodes as shown in Fig. 2.5. By sending regular pulses of electrical signal via vagus nerve, VNS system can suppresses epileptic seizure before seizure happens. Currently, VNS is approved by Food and Drug Administration (FDA). Other electrical treatments have also been researched such as deep brain stimulation (DBS) shown in Fig. 2.6 [20], [21].

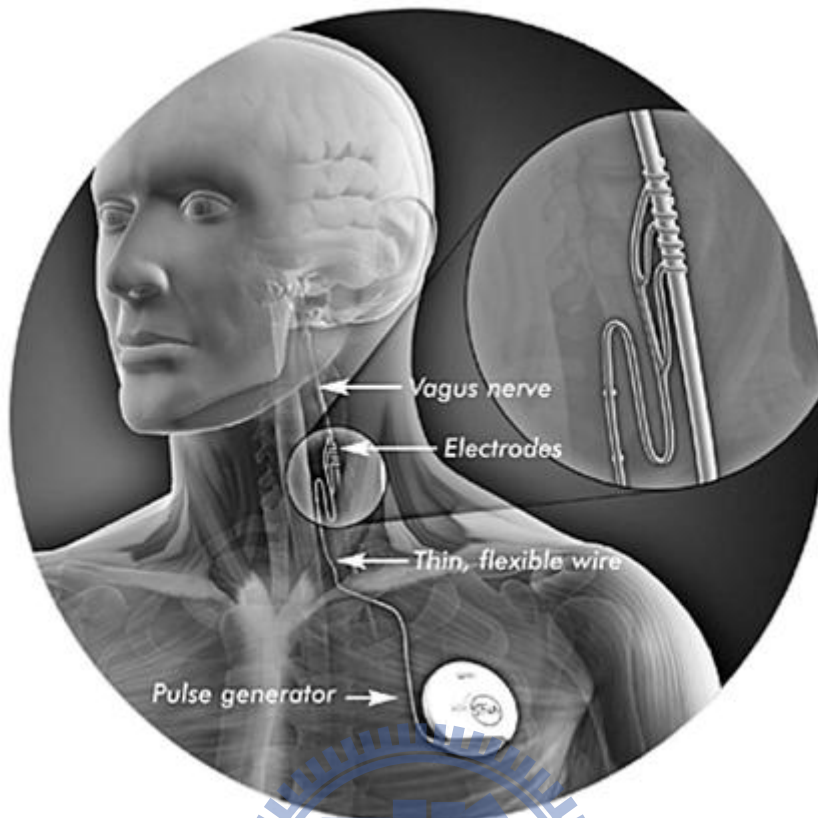


Fig. 2.5. Vagus nerve stimulation [18].

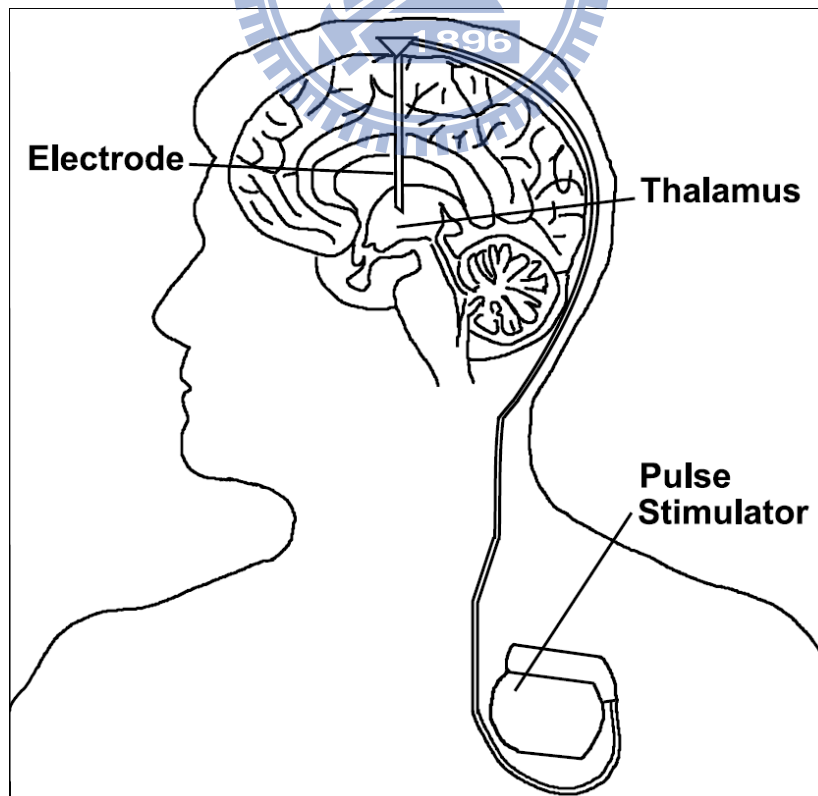


Fig. 2.6. Deep brain stimulation [20].

2.2.2 Epileptic Seizure Detecting and Controlling System

In recent decades, as bioelectronics developed, epileptic seizure becomes predictable by detecting and analyzing EEG in time or frequency domains [22], [23], [24]. Several methods to predict epileptic seizure such as predictable features, prediction by classification, and entropy calculation have been researched [25]. It has also been demonstrated that the abnormal discharge signal that causes epileptic seizure can be suppressed by TES before seizure happens. A variety of epileptic seizure detecting and controlling systems has been studied and implemented. The systems for epileptic treatment can be mainly classified into open-loop systems and closed-loop systems [26].

Open-loop systems, which are also called blind systems, are not able to respond to physiological activities immediately. The neuroscientists intend to modulate seizure by activating and inactivating regions and set the required stimulus current for individual region. Open-loop systems regularly turn on and off at a fixed pattern which is determined by neuroscientists before the event. Almost all of the currently existing systems that have been approved by FDA adopt open-loop systems [19]. Closed-loop systems, which are also called intelligent systems, are more complicated because they are able to respond to physiological activities immediately. The systems are switched on only when the physiological signals of epileptic seizure are detected. To be compared with open-loop systems, closed-loop systems can stimulate the location of seizure only and hence minimize the effect to human body. Closed-loop systems are consisted of detector, signal analyzer, controller, and stimulus driver.

As current researches shown, the seizure of epilepsy can be traced back to tens of seconds before onset by the EEG, which means that when the seizure-like brainwave is detected, there is still up to 10 seconds remained before the epileptic seizure happens [27]. During this time, the use of closed-loop systems may be effective to deal with

epileptic seizure. Therefore, a number of algorithms have been proposed for rapidly detecting and classifying the sign of different kinds of epileptic seizure. These algorithms analyze the brain activities recorded from EEG or electrocorticogram (ECoG) and extract the features of seizure-like brainwave, and the outcome of analysis can be utilized to decide whether to provide TES or not. Due to the complexity of closed-loop systems, power consumption is also one of mainly considerations while being applied to implantable systems. Fig. 2.7 shows a closed-loop epileptic seizure monitor and controller presented in 2011 [28].

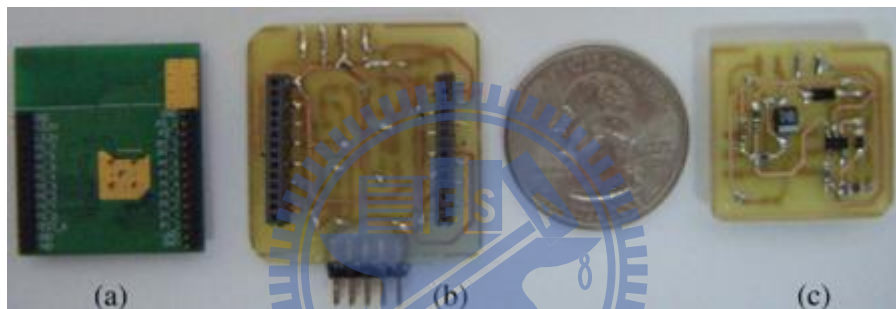


Fig. 2.7. The closed-loop epileptic seizure monitor and controller system consisted of (a) microcontroller board, (b) signal conditioning board, and (c) stimulator board [28].

2.3 Brief Introduction of Implantable Stimulus Driver Technique

Therapeutic electrical stimulation (TES) and functional electrical stimulation (FES) have been developed and implemented for a variety of applications in medical science and clinical trials. In the past, some diseases were considered too difficult to be cured such as the retinitis pigmentosa (RP) [2], Alzheimer's disease [29], and the damage of central nervous system. In the recent years, these diseases may become curable by TES. Thus a variety of implantable stimulus drivers have been researched and presented in order to provide stimulus current for TES. While designing implantable stimulus drivers,

there are many considerations that must be taken into account such as safety, reliability, voltage compliance, power consumption, charge balance, and density of stimulus sites. In this subsection, some previous works of stimulus drivers with different design considerations are briefly introduced. Both their advantages and disadvantages are mentioned as well.

Fig. 2.8 shows the stimulus driver with blocking-capacitor proposed in 2006 [30]. Some irresistible factors may cause the damage of implanted devices such as moisture. A failure in output stage of implanted device may lead to prolonged dc current flowing from stimulus driver to human body and result in serious damage. For the consideration of safety, the use of off-chip blocking-capacitor in output stage of stimulus drivers is adopted. By the use of blocking-capacitor, the prolonged dc current flowing from stimulus driver to human body can be prevented. However, the size of capacitors is too large, and capacitors usually dominate the size of implantable stimulus driver.

To improve the disadvantage mentioned above, the technique pronounced in 2006 utilized two complementary current sources to deliver stimulus current [30]. By delivering stimulus current through one capacitor and discharging accumulated charge on the other capacitor, the purpose to deliver complementary stimulus current is achieved. In this way, the size of blocking-capacitor is reduced by the ratio of switching rate of the two current sources. Thus, reduced capacitors can be integrated into implantable stimulus driver. Despite the disadvantage of large size can be improved, there are still problems while using blocking-capacitors. The blocking-capacitors provide output stage of stimulus driver with extra voltage drop, so the required operating voltage of the circuit is higher. It directly decreases voltage compliance of the circuit.

The stimulus driver delivers stimulus current through electrodes into the tissue. While stimulus current is conducted, chemical process may occur at the electrode-tissue

interface. Some studies revealed that unbalanced stimulus current may cause net charge to store in body and lead to destructive problems such as electrolysis, gazing, pH changing, and dissolution [31], [32]. In order to solve these problems, some bi-phase stimulus drivers have been presented. The purpose of these works is to generate balanced current of anodic pulse and cathodic pulse [33].

There are many other considerations while designing implantable stimulus driver. In order to provide constant stimulus current irrespective of high variety of loading impedance, stimulus driver of high output impedance should be considered. Fig. 2.9 [33] shows the improved current sources with fully cascaded structure which provides high impedance at the output. Another stimulus driver with voltage controlled resistors (VCR) current source shown in Fig. 2.10 [34] utilizes MOS transistors operating in deep triode region to gain the voltage compliance close to the fixed power supply. Indeed, while designing a stimulus driver, it is rare that just one of the considerations is taken into account [35]. This work investigates stimulus driver for epileptic seizure control with considerations of reliability, safety, variation of tissue impedance, and power consumption.

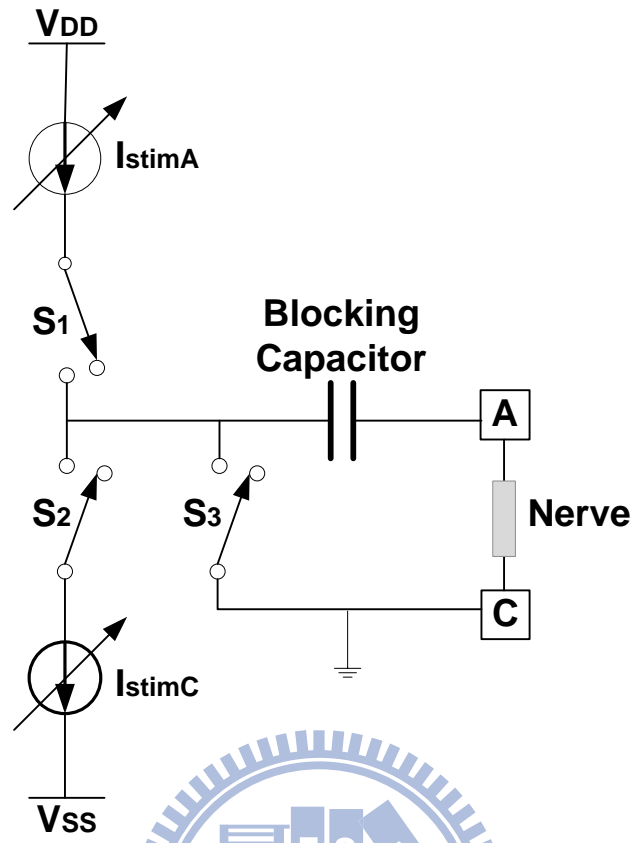


Fig. 2.8. Stimulator output stage with blocking capacitor [30].

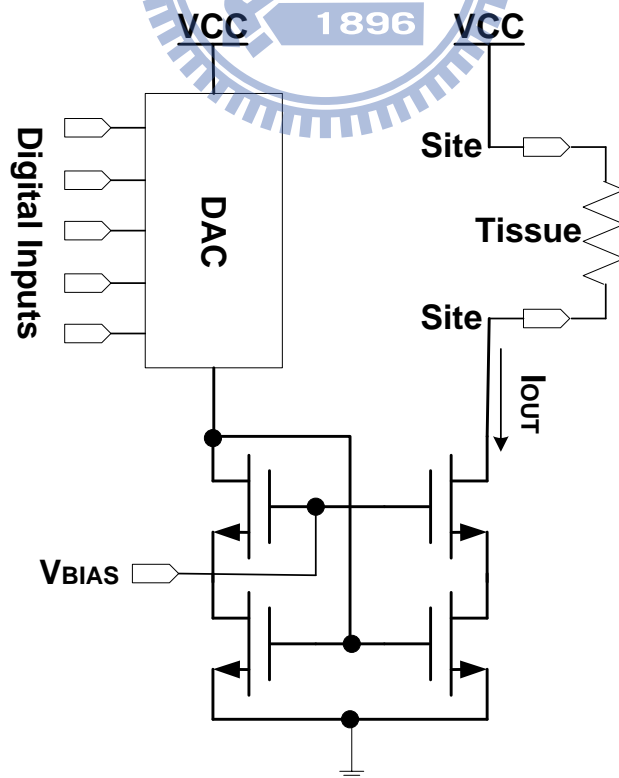


Fig. 2.9. Wide swing cascode current source of stimulator [33].

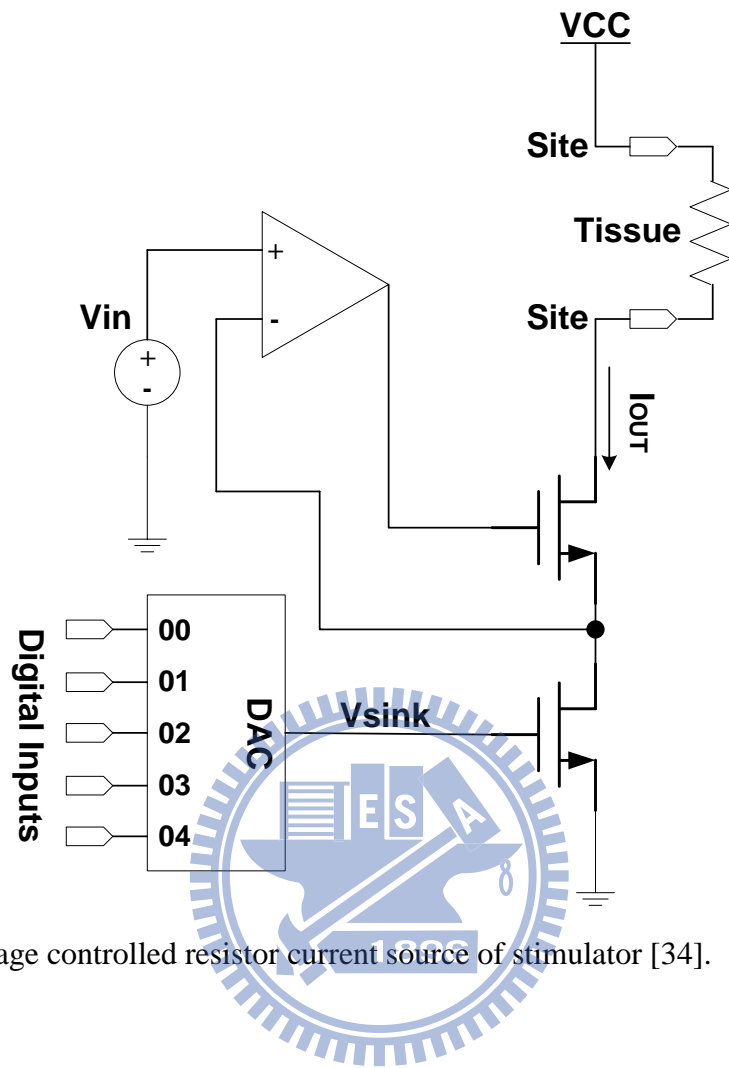


Fig. 2.10. Voltage controlled resistor current source of stimulator [34].

Chapter 3

Design of High-Voltage-Tolerant Stimulus Driver to Suppress Epileptic Seizure with Adaptive Loading Consideration in 0.18- μm CMOS Process

3.1 Introduction

Epilepsy is one of the most common neurological disorder that caused by abnormal discharge in brain. Traditional therapies include pharmacologic treatment and surgical treatment. Pharmacologic treatment is the most common used. For patients who do not respond to the medicament, non-reversible brain surgery is in common use. But the risky surgery may cause functional loss. Furthermore, only 75% do response to traditional therapies [5]. In recent years, functional electrical stimulation (FES) and therapeutic electrical stimulation (TES) have been demonstrated that can restore some physical functions of a human. Epilepsy is also one of diseases investigated to be treated by therapeutic electrical stimulation. Nowadays, epileptic seizure becomes predictable by detecting premonition of epileptic seizure from electroencephalography (EEG) or electrocorticogram (ECoG) in time or frequency domains. It has been demonstrated that the epileptic seizure caused by abnormal discharge signals can be suppressed by electrical stimulation before seizure happens. Compare to non-reversible surgical treatment, the advantages of electrical stimulation therapies are harmless to the tissue of the brain. Besides, it can make adjustment arbitrarily and is more flexible. As the

transistor size reduces in CMOS technology, devices can integrate into a chip that is implantable. Fig. 3.1 shows the block diagram of an implantable stimulus driver system for epileptic treatment.

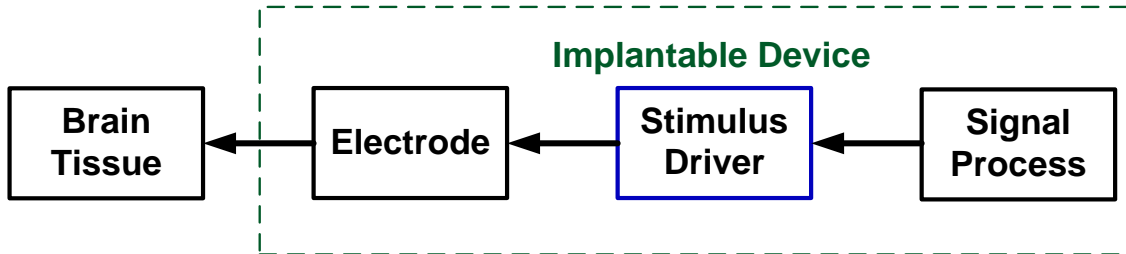


Fig. 3.1. The block diagram of an implantable stimulus driver for epilepsy treatment.

Due to different kinds of tissue, locations, and implanted time, the equivalent impedance of electrode and tissue will vary in a wide range. The tissue impedance for individuals ranges from tens $k\Omega$ to hundreds $k\Omega$ [28]. According to the specifications derived from experimental demand, the range of stimulus current, which is able to suppress epileptic seizures without being harmful to the rats, is within $35 \mu A$ to $50 \mu A$. The output current of this proposed stimulus driver is then set to fit the specification. The equivalent tissue impedance is within $100 k\Omega$ to $250k\Omega$. By multiplying tissue impedance by stimulus current, high voltage ($\sim 10 V$) occurs at the output of stimulus driver. To prevent reliability issues, using some special structures to sustain the high voltage is needed [36] – [40]. To an implantable device, power consumption is also an important consideration. With the considerations of reliability, safety, and power consumption, the stimulus driver used in the implantable device for seizure control is investigated in this work. The detailed circuit simulation and measurement results of the proposed design will be presented in the following sections.

3.2 Novel High-Voltage-Tolerant Stimulus Driver with Adaptive Loading Consideration Fabricated in 0.18- μm CMOS Process

3.2.1 Implementation

Fig. 3.2 shows the block diagram of proposed stimulus driver, which contains charge pump system, output driver, and V_{CC} control circuit. The output driver receives the system supply voltage (V_{DD}), stimulation signal (V_{ST}), and variable operating voltage (V_{CC}), and then delivers the stimulus current to the load (electrode/tissue). The V_{CC} control circuit detects the stimulus current, and then sends the control signals (A and B) to the charge pump system. The charge pump system receives the clock signal, system supply voltage (V_{DD}), stimulation signal (V_{ST}), and the control signals (A and B), and then delivers variable operating voltage (V_{CC}) depending on the loading impedance. In this work, output driver and V_{CC} control circuit are implemented.

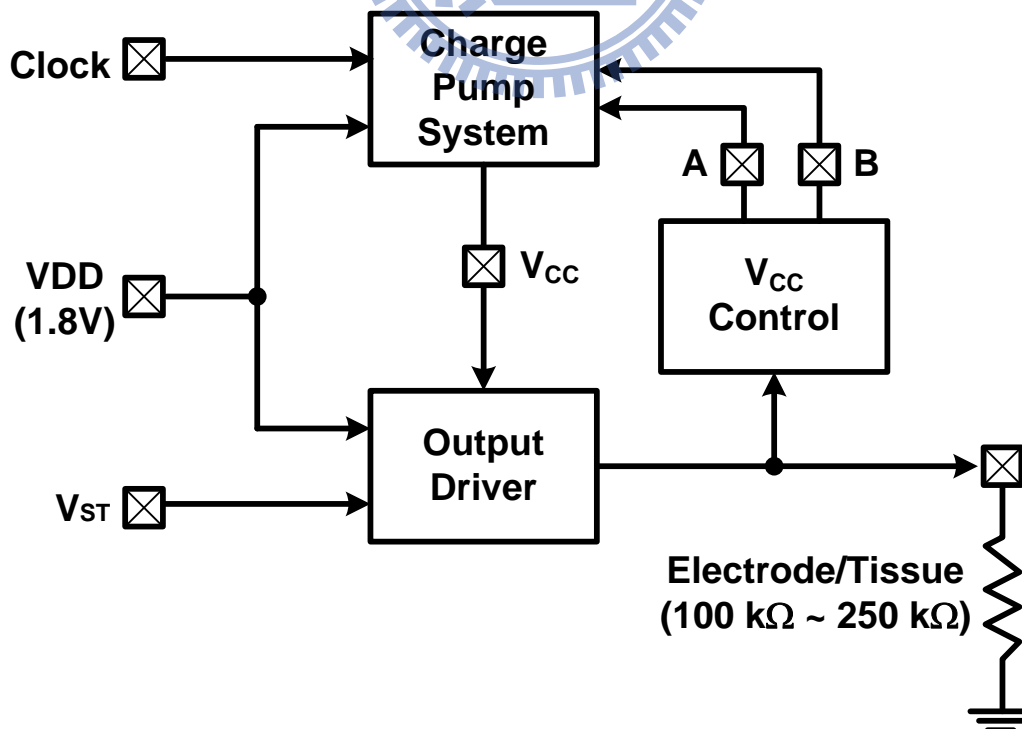


Fig. 3.2. Block diagram of the proposed stimulus driver.

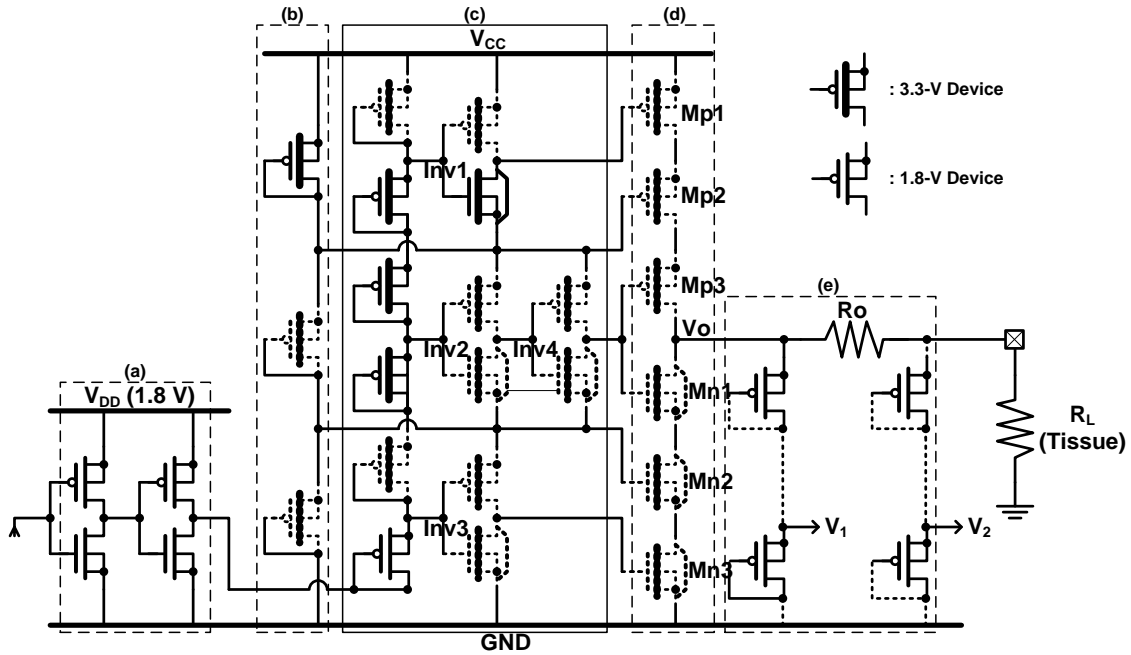


Fig. 3.3. Structure of output driver fabricated in 0.18- μm 1.8-V/3.3-V CMOS process. 3.3-V transistors are shown with thick gate oxide, and 1.8-V transistors are shown with thin gate oxide.

The output driver circuit fabricated in 0.18- μm CMOS process is shown in Fig. 3.3. Both 3.3-V transistors (shown with thick gate oxide) and 1.8-V transistors (shown with thin gate oxide) are used. In order to sustain the high voltage ($\sim 10\text{V}$) without gate-oxide overstress, the stacked MOS configuration with 3.3-V transistors between V_{cc} and ground is used. The output driver can be divided into five parts: input buffer, bias circuit, control circuit, output stage, and detection circuit. The input buffer is used to provide a full-swing of 1.8 V while receiving the stimulation signal (V_{ST}). The bias circuit, which consists of three PMOS diodes, is used to provide the biases of $2V_{cc}/3$ and $V_{cc}/3$. The control circuit, which is made up of a PMOS-diode chain and four inverters, plays the role of a level shifter. When V_{ST} is high, the voltage at the bottom of the PMOS-diode chain is 1.8 V. Through the PMOS-diode chain, all the input voltages of the three inverters Inv1, Inv2, and Inv3 equal to logic “1,” and the input voltage of Inv4 equals to logic “0.” In this condition, the output voltages of Inv1, Inv4, and Inv3 are $2V_{cc}/3$, $2V_{cc}/3$, and 0 V, respectively. The gate voltages of Mp1, Mp2, Mp3, Mn1, Mn2, and

Mn3 are $2V_{cc}/3$, $2V_{cc}/3$, $2V_{cc}/3$, $2V_{cc}/3$, $V_{cc}/3$, and 0 V, respectively. Mp1, Mp2, and Mp3 are turned on to transfer stimulus current, and all the drain voltages of them almost equal to V_{cc} . Mn1, Mn2, and Mn3 are turned off, and drain voltages of them are V_{cc} , $2V_{cc}/3$, and $V_{cc}/3$, respectively. When V_{ST} is low, the voltage at the bottom of the PMOS-diode chain is 0 V. Through the PMOS-diode chain, all the input voltages of the three inverters Inv1, Inv2, and Inv3 equal to logic “0,” and the input voltage of Inv4 equals to logic “1.” In this condition, the output voltages of Inv1, Inv4, and Inv3 are V_{cc} , $V_{cc}/3$, and $V_{cc}/3$, respectively. The gate voltages of Mp1, Mp2, Mp3, Mn1, Mn2, and Mn3 are V_{cc} , $2V_{cc}/3$, $V_{cc}/3$, $V_{cc}/3$, $V_{cc}/3$, and $V_{cc}/3$, respectively. Mn1, Mn2, and Mn3 are turned on to discharge the output node V_o , and all the drain voltages of them equal to 0 V. Mp1, Mp2, and Mp3 are turned off, and drain voltages of them are $2V_{cc}/3$, $V_{cc}/3$, and 0 V, respectively. For both the cases V_{ST} is high or low, the max voltage of $|V_{GS}|$, $|V_{DS}|$, and $|V_{GD}|$ is $V_{cc}/3$. The max voltage drop across a 3.3-V device is 3.12V because the max operating voltage V_{cc} here we use is 9.36 V. So there is no gate-oxide overstress happened. Fig. 3.4 to Fig. 3.7 show the voltage conditions of each node of the output driver in four different operating regions of $V_{cc} = 5.04$ V, 6.48 V, 7.92 V, and 9.36 V, respectively. The stimulation is controlled by the 1.8-V signal (V_{ST}). Whether the stimulation is turned off or on, all voltage differences across the MOS transistors are lower than their sustainable voltages (1.8 V or 3.3 V) to prevent reliability issues. The detection circuit is consisted of two PMOS-diode chains and one output resistor. The output resistor ($R_o = 2$ k Ω) is arranged before the electrode and the tissue. When the stimulus current flows through R_o , a voltage drop across R_o occurs. Two PMOS-diode chains connected to each end of R_o are used to generate biases V_1 and V_2 . As the value of V_1 lies in the value of V_{cc} , the value of V_2 lies in both the value of V_{cc} and the stimulus current (I_{stim}). The voltage difference between V_1 and V_2 can be distinguished by comparators.

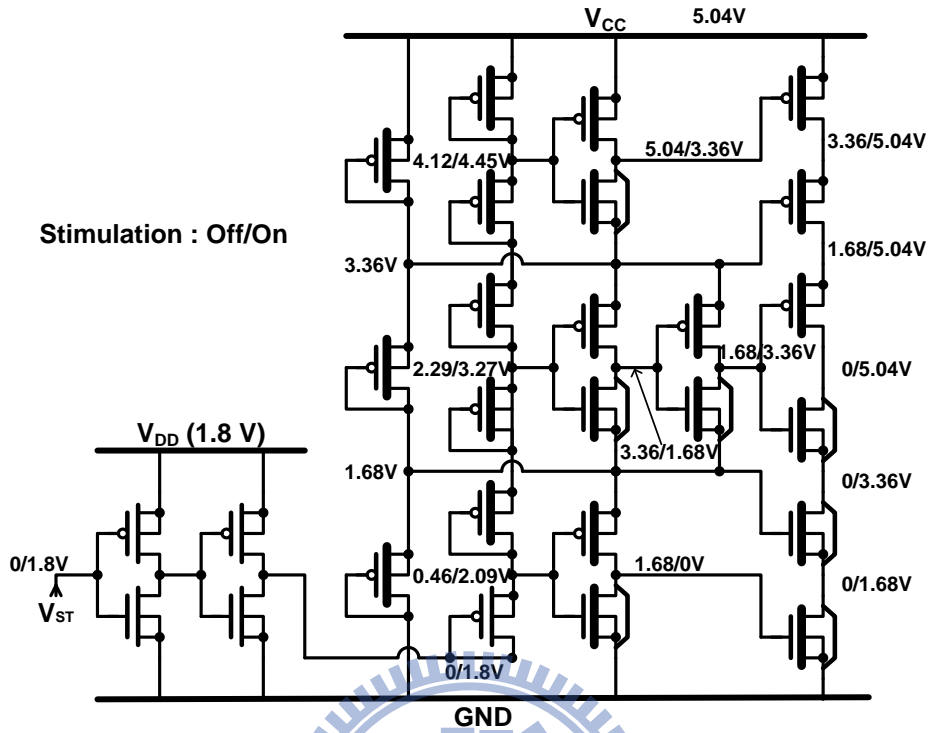


Fig. 3.4. Voltage conditions of each node in output driver circuit as operating voltage $V_{cc} = 5.04$ V.

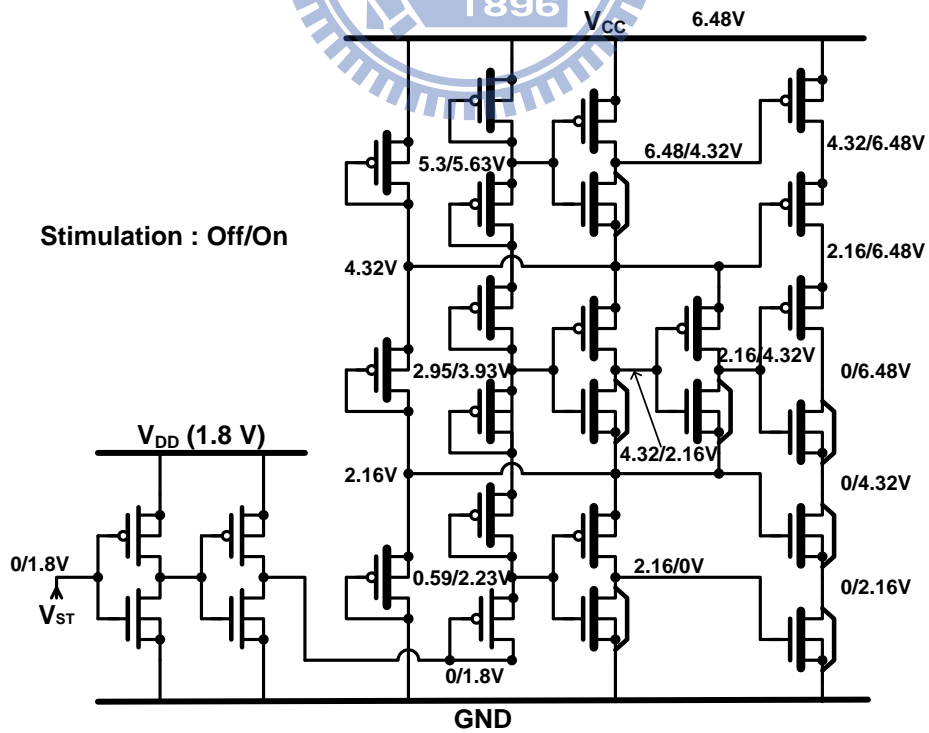


Fig. 3.5. Voltage conditions of each node in output driver circuit as operating voltage $V_{cc} = 6.48$ V.

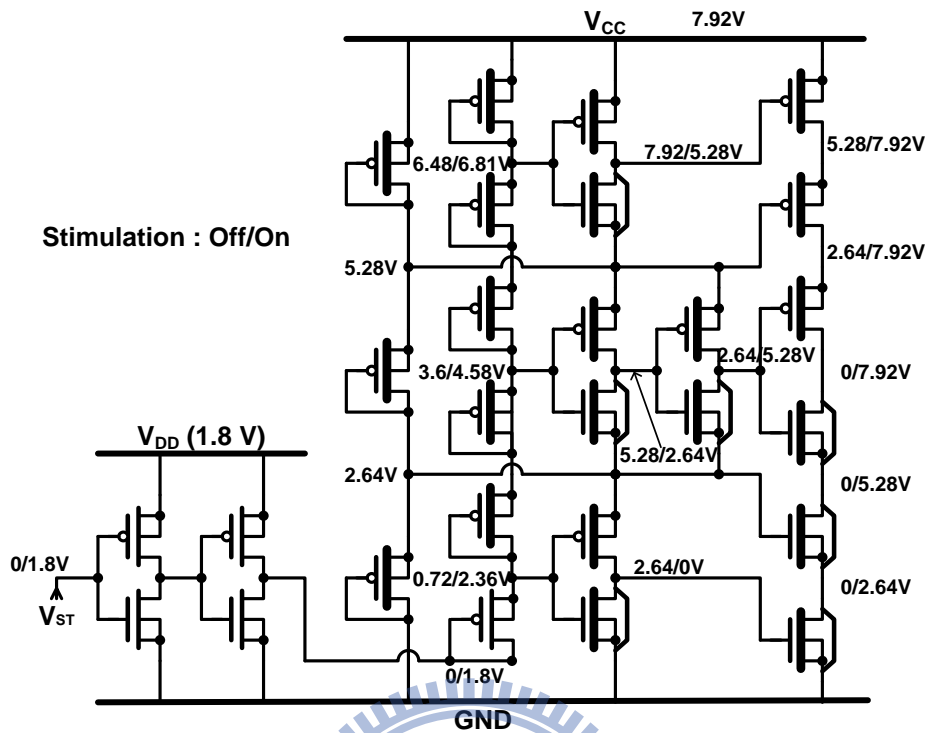


Fig. 3.6. Voltage conditions of each node in output driver circuit as operating voltage $V_{cc} = 7.92$ V.

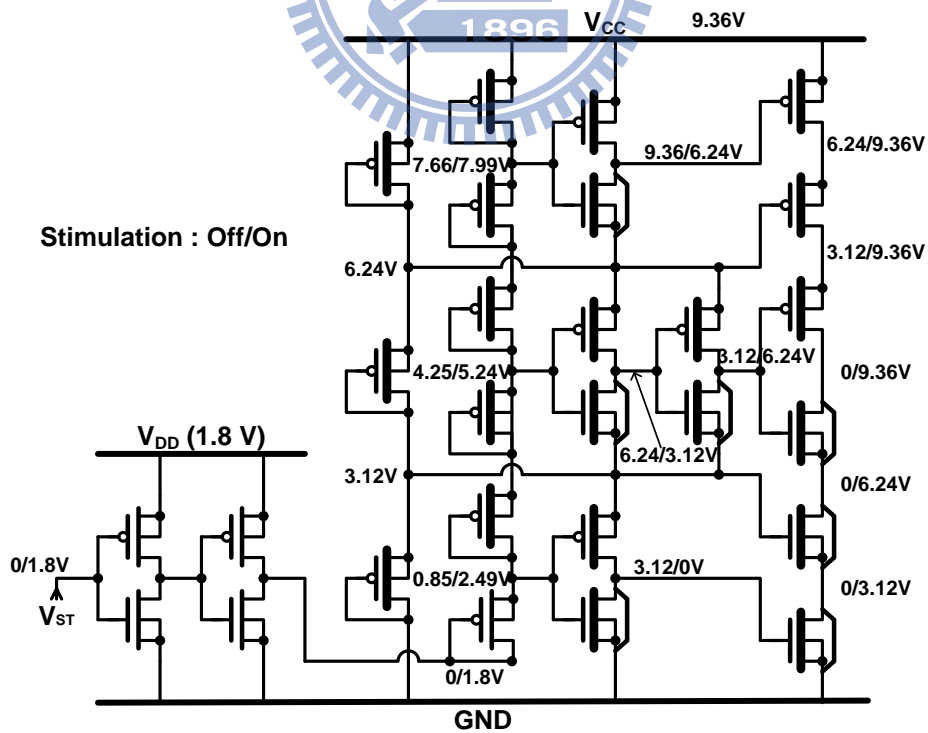


Fig. 3.7. Voltage conditions of each node in output driver circuit as operating voltage $V_{cc} = 9.36$ V.

The purpose of V_{cc} control circuit is to generate control signals, so the charge pump system can generate a corresponding value of operating voltage V_{cc} according to the present control signals. In this work, we desire to generate four levels of V_{cc} (5.04, 6.48, 7.92, and 9.36 V), so control signals of two bits A/B are required. The V_{cc} control circuit consists of three comparators (C1, C2, and C3) and logic gates circuit as shown in Fig. 3.8. Here we transfer V1 and V2, which are derived from detection circuit of output driver, to the inputs of these three comparators. Fig. 3.9 shows the structure of the comparators, each of them consists of a differential pair (M1 and M2), a current mirror (M3 and M4), a resistor (R_s), a current source (M5), and an inverter (M6 and M7).

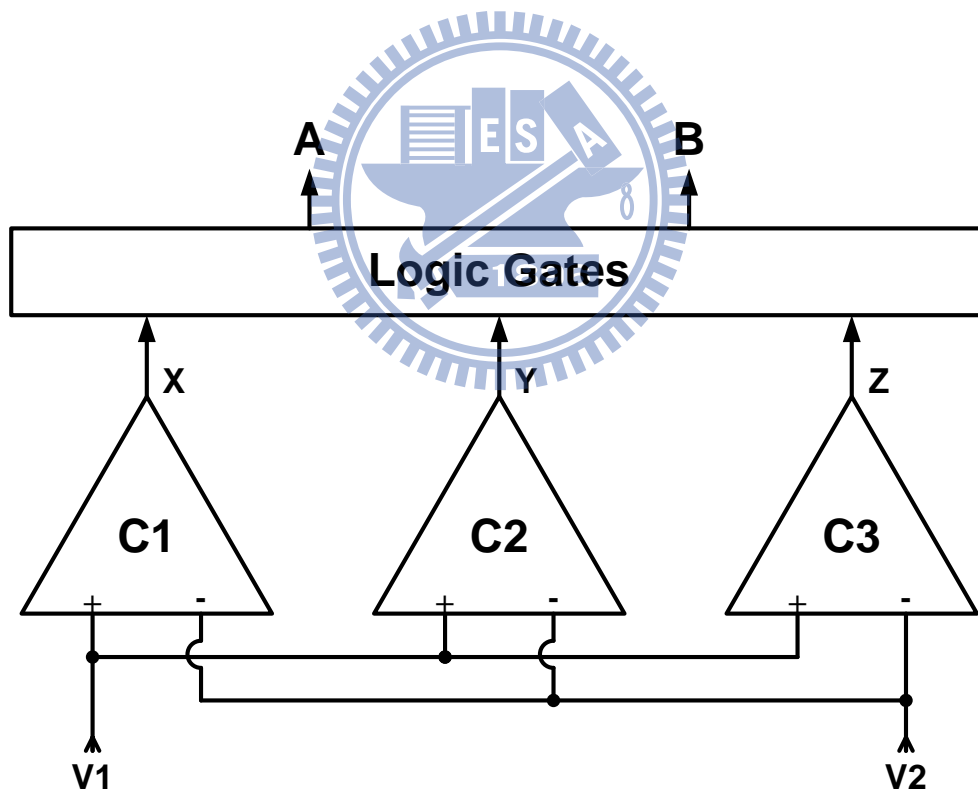


Fig. 3.8. The V_{cc} control circuit consisted of three comparators and logic gates.

specification. At this operating point (here we choose $R_L = 130 \text{ k}\Omega$), V_{cc} should be changed to a higher level in order to provide enough stimulus current. By selecting a proper value of R_s , we can make the output of comparator C1 change from logic “0” to “1” when the loading impedance reaches the value $R_L = 130 \text{ k}\Omega$. Consider that when V_{cc} changes from 5.04 V to 6.48 V due to the output of C1 changing from “0” to “1,” the stimulus current is raised as well. Raised I_{stim} through R_o makes the voltage difference between V1 and V2 become larger. If the current flowing through R_s can’t be enlarged simultaneously, the output of C1 will change back to “0,” and then will vary between “0” and “1” repeatedly. In order to avoid this unstable condition, it is necessary to enlarge the current through R_s when V_{cc} changes to a high level. We notice that not only the differential voltage between V1 and V2 rises with increased V_{cc} , but also the common-mode voltage does. There are two ways to enlarge the current through R_s as the common-mode voltage is raised: one is to replace M5 by a resistor, and the other is to operate M5 in triode region at the beginning. The second method is adopted here because it occupies less layout area and consumes less power than the first method. The reason why it consumes less power is that when V_{cc} changes to a higher level again (from 6.48 V to 7.92 V), by using a resistor to replace M5 as the current source, the current flowing through the current source will rise again. If M5 is designed to turn from triode region into saturation region at the first time V_{cc} increases, then the current through M5 won’t rise obviously at the second time V_{cc} increases. Hence it has less power consumption than using a resistor. As the comparator C1 is designed to change V_{cc} from 5.04 V to 6.48 V, C2 and C3 are designed to change V_{cc} from 6.48 V to 7.92 V and from 7.92 V to 9.36 V, and each M5 of them turns from triode region into saturation region in the meantime V_{cc} changes. The corresponding operating points to change V_{cc} from 6.48 V to 7.92 V and from 7.92 V to 9.36 V are $R_L = 170 \text{ k}\Omega$ and $R_L = 210 \text{ k}\Omega$. Table 3.1 shows the relations among V1 and V2 of output driver, outputs of

comparators X/Y/Z, desired control signals A/B, and corresponding V_{cc}. According to Table 3.1, The K-map shown in Fig. 3.10 can be drawn. The logic gates circuit to generate control signals A/B can be accomplished by deriving Eq. (3-1) and (3-2) from the K-map.

$$A = Y \quad (3-1)$$

$$B = XZ' \quad (3-2)$$

The logic gates circuit corresponding to Eq. (3-1) and (3-2) are shown in Fig. 3.11.

Table 3.1. Relationship of V₁, V₂, comparator outputs, control signals, operating voltage, and reference voltage.

V ₁	V ₂	X	Y	Z	A	B	V _{CC}	V _{ref} = V _{CC} /6
0.611 V	< 0.602 V	0	0	0	0	0	5.04 V	0.84 V (V _{DD} * 7/15)
0.796 V	< 0.787 V	1	0	0	0	1	6.48 V	1.08 V (V _{DD} * 9/15)
0.978 V	< 0.969 V	1	1	0	1	1	7.92 V	1.32 V (V _{DD} * 11/15)
1.159 V	—	1	1	1	1	0	9.36 V	1.56 V (V _{DD} * 13/15)

↖ V₂ > 0.602 V
 ↖ V₂ > 0.787 V
 ↖ V₂ > 0.969 V

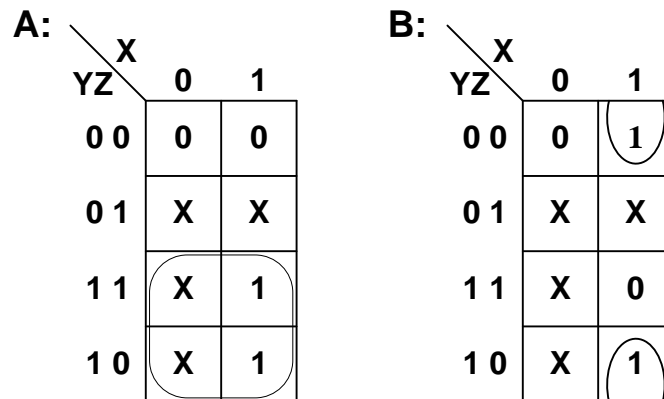


Fig. 3.10. K-map of control signals A and B derived from Table 3.1.

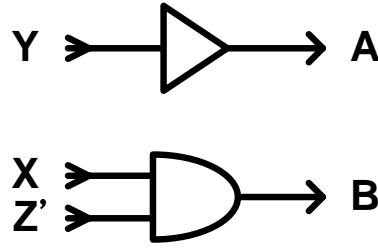


Fig. 3.11. The related logic gates of Eq. (3-1) and (3-2).

The Vcc control circuit behaves like a state machine to send out control signals A/B as 0/0→0/1→1/1→1/0 with corresponding outputs of comparators X/Y/Z as 0/0/0→1/0/0→1/1/0→1/1/1. At the beginning of the stimulation condition, X/Y/Z are 0/0/0, A/B are 0/0, and 5.04-V Vcc is delivered to the output driver initially. If the loading impedance (R_L) is within 100 k Ω to 130 k Ω , X/Y/Z, A/B, and Vcc keep their origin values. If the loading impedance is higher than 130 k Ω , 170 k Ω , and 210 k Ω , the A/B signals become 0/1, 1/1, and 1/0, respectively with corresponding comparators outputs 1/0/0, 1/1/0, and 1/1/1. In the mean time, 6.48-V, 7.92-V, and 9.36-V Vcc are delivered to the output driver. After the stimulation condition, the stimulus driver is turned off, and control signals A/B are reset to 0/0.

The charge pump system is shown in Fig. 3.12 [41], which contains a reference voltage selector (V_{ref} selector) shown in Fig. 3.13. From Table 3.1, the ratio of resistors in the V_{ref} selector can be derived as shown in Eq. (3-3), and the output voltage of the V_{ref} selector (V_{ref}) equals $7V_{DD}/15$ (0.84V), $9V_{DD}/15$ (1.08V), $11V_{DD}/15$ (1.32V), or $13V_{DD}/15$ (1.56V), according to the control signals A/B = 0/0, 0/1, 1/1, 1/0, respectively .

$$r1 : r2 : r3 : r4 : r5 = 7 : 2 : 2 : 2 : 2 \quad (3-3)$$

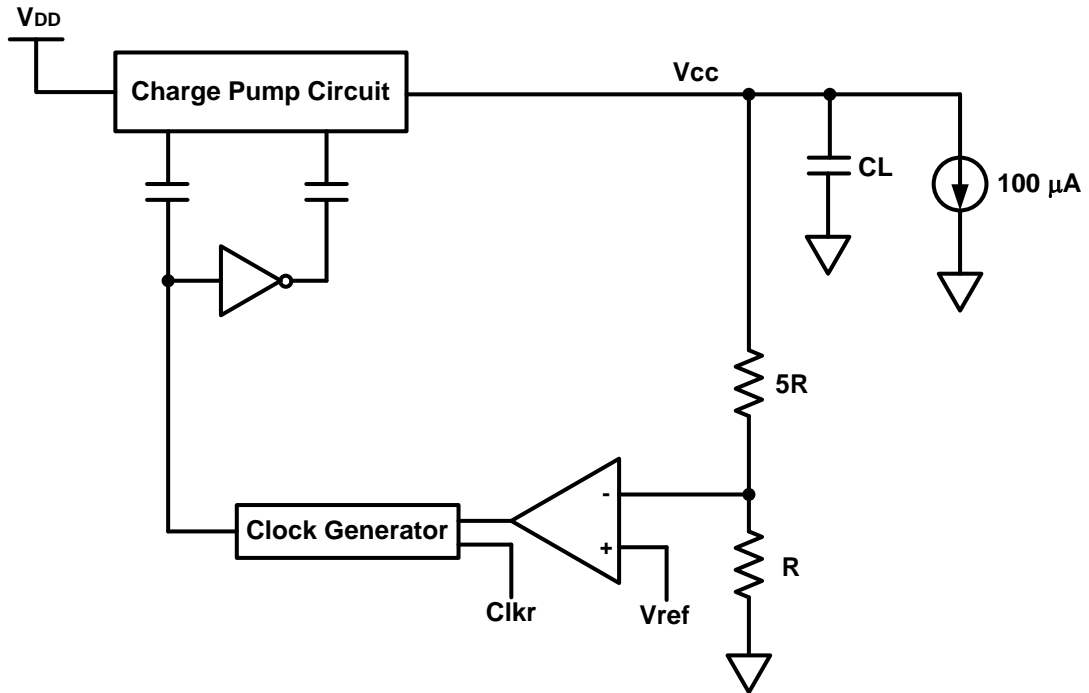


Fig. 3.12. The charge pump system.

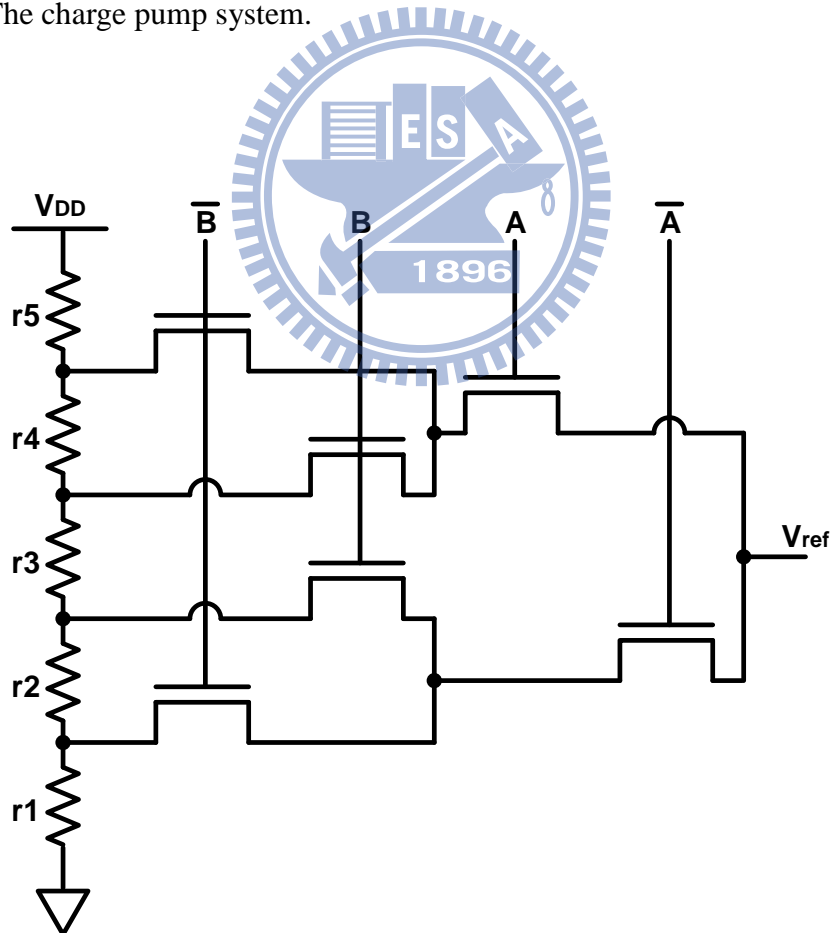
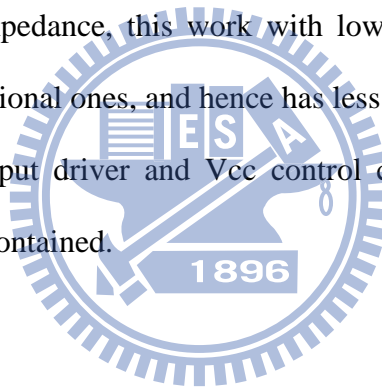


Fig. 3.13 Reference voltage selector in the charge pump system. With selected r1 ~ r5, the value of V_{ref} depends on control signals A and B.

Once the control signals are decided, the corresponding V_{ref} is delivered to the comparator (V_+) shown in Fig. 3.12. The other input of the comparator (V_-) is $V_{cc}/6$. If $V_{cc}/6$ is smaller than V_{ref} , the output of comparator is “1,” the clock generator activates charge pump circuit and V_{cc} increases. When $V_{cc}/6$ becomes slightly larger than V_{ref} , the charge pump circuit keeps delivering steady V_{CC} by means of the feedback loop in the charge pump system. Fig. 3.14 shows the operating voltage V_{cc} of proposed stimulus driver verses tissue impedance. Operating voltage of conventional design is also contained in Fig. 3.14 to be compared. The proposed stimulus driver operates at four different levels of V_{cc} in accordance of loading impedance while conventional works operating with fixed operating voltage. For the condition of fixed stimulus current and low loading impedance, this work with lower operating voltage is more power efficient than conventional ones, and hence has less power consumption.

In this work, only output driver and V_{cc} control circuit are implemented. The charge pump system is not contained.



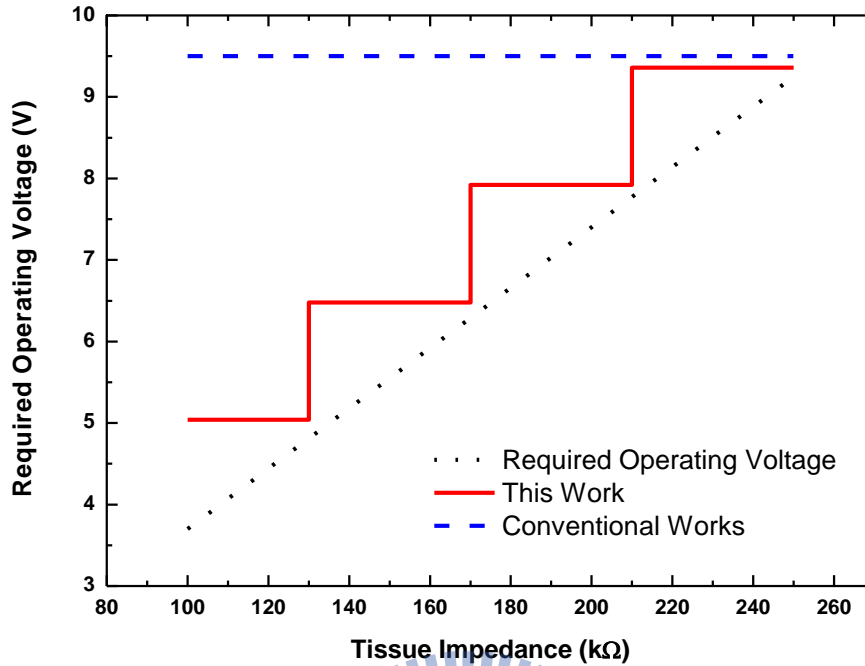
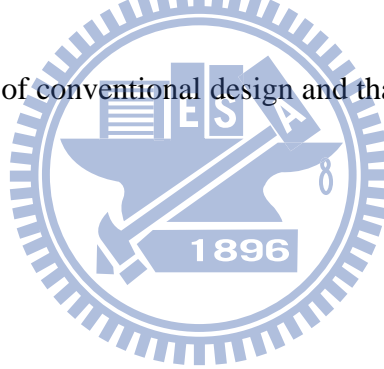


Fig. 3.14. Operating voltage of conventional design and that of proposed stimulus driver verses tissue impedance.



3.2.2 Simulation Results

Fig. 3.15 to Fig. 3.18 show how to decide the correct level of V_{cc} with corresponding tissue impedance by simulation results while simulating, and the upper limit tissue impedance of this design ($R_L = 250 \text{ k}\Omega$) is adopted here. At the beginning, V_{cc} is set to be 5.04 V originally, stimulus current $I_{stim} = 19.69 \mu\text{A}$, and control signals $A/B = 0/1$ as shown in Fig. 3.15. With corresponding to $A/B = 0/1$, V_{cc} should be set to 6.48 V, and then repeat the simulation. The simulation results for $V_{cc} = 6.48 \text{ V}$ are $I_{stim} = 25.42 \mu\text{A}$, and control signals $A/B = 1/1$ as shown in Fig. 3.16. With corresponding to $A/B = 1/1$, V_{cc} should be change to 7.92 V, and then repeat the simulation. The simulation results for $V_{cc} = 7.92 \text{ V}$ are $I_{stim} = 31.12 \mu\text{A}$, and control signals $A/B = 1/0$

as shown in Fig. 3.17. Simulation should be repeat again with $V_{cc} = 9.36$ V since $A/B = 1/0$. The simulation results for $V_{cc} = 9.36$ V are $I_{stim} = 36.82$ μ A, and control signals $A/B = 1/0$ as shown in Fig. 3.18. From the simulation results, the control signals A/B maintain the same values as that of $V_{cc} = 7.92$ V, which means the present value of V_{cc} is suitable for $R_L = 250$ k Ω , and the stimulus current with sufficient magnitude is provided by the stimulus driver. The simulation results of stimulus current as loading impedance $R_L = 100$ k Ω and 250 k Ω with their corresponding V_{cc} are shown in Fig. 3.19.

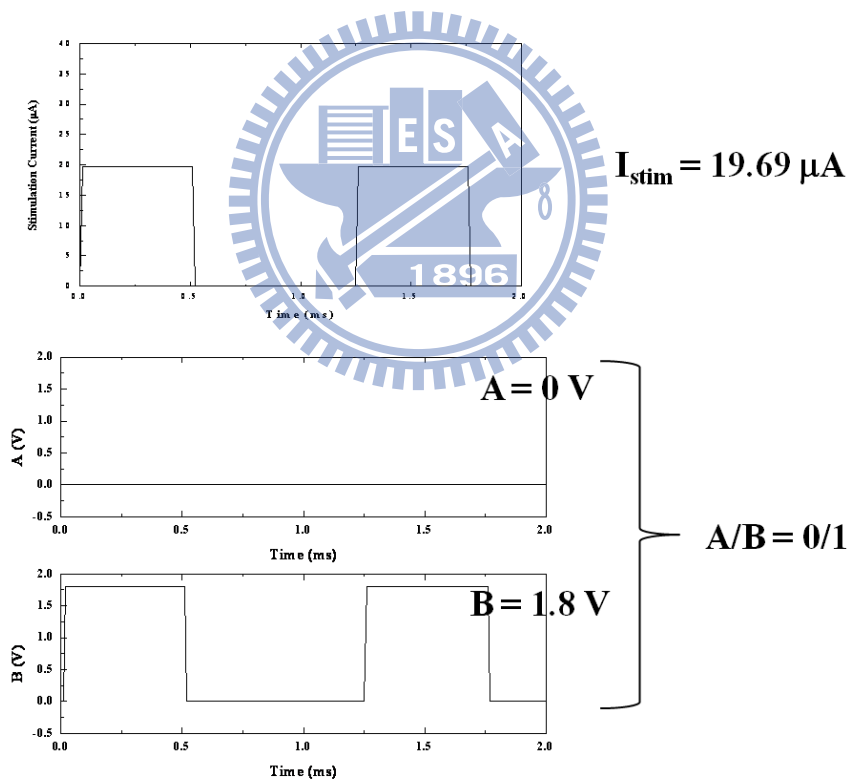


Fig. 3.15. The simulation results of stimulus current and control signals as loading impedance $R_L = 250$ k Ω and operating voltage $V_{cc} = 5.04$ V.

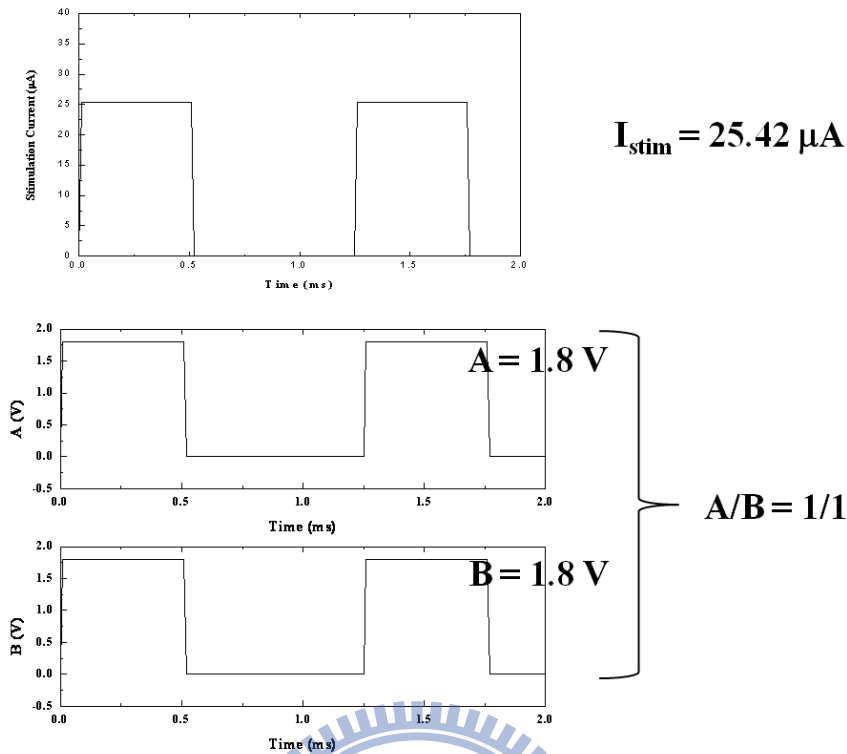


Fig. 3.16. The simulation results of stimulus current and control signals as loading impedance $R_L = 250 \text{ k}\Omega$ and operating voltage $V_{cc} = 6.48 \text{ V}$.

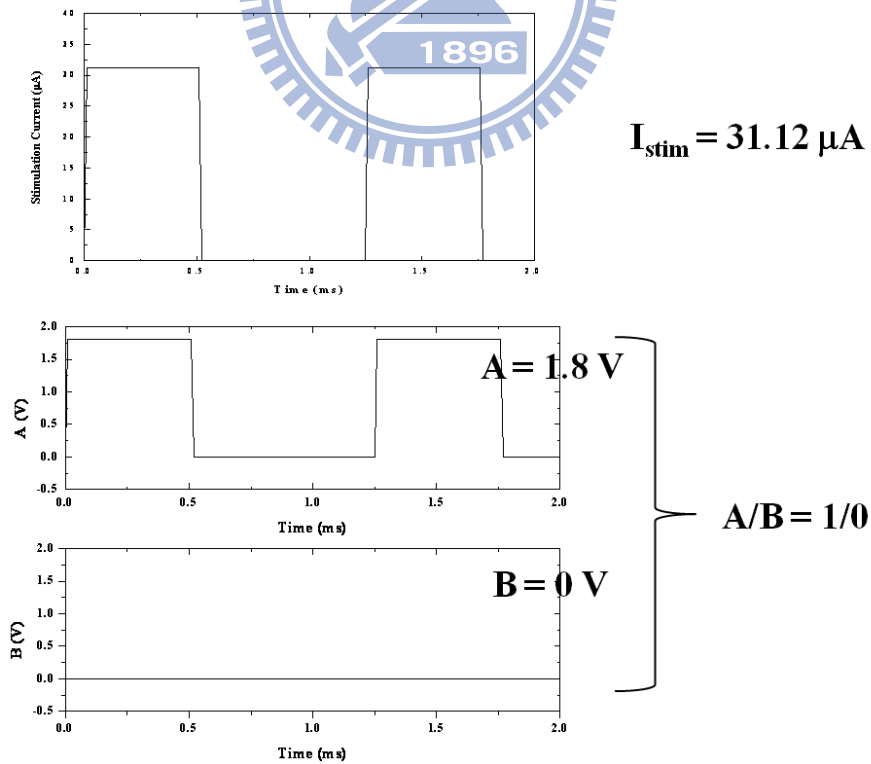


Fig. 3.17. The simulation results of stimulus current and control signals as loading impedance $R_L = 250 \text{ k}\Omega$ and operating voltage $V_{cc} = 7.92 \text{ V}$.

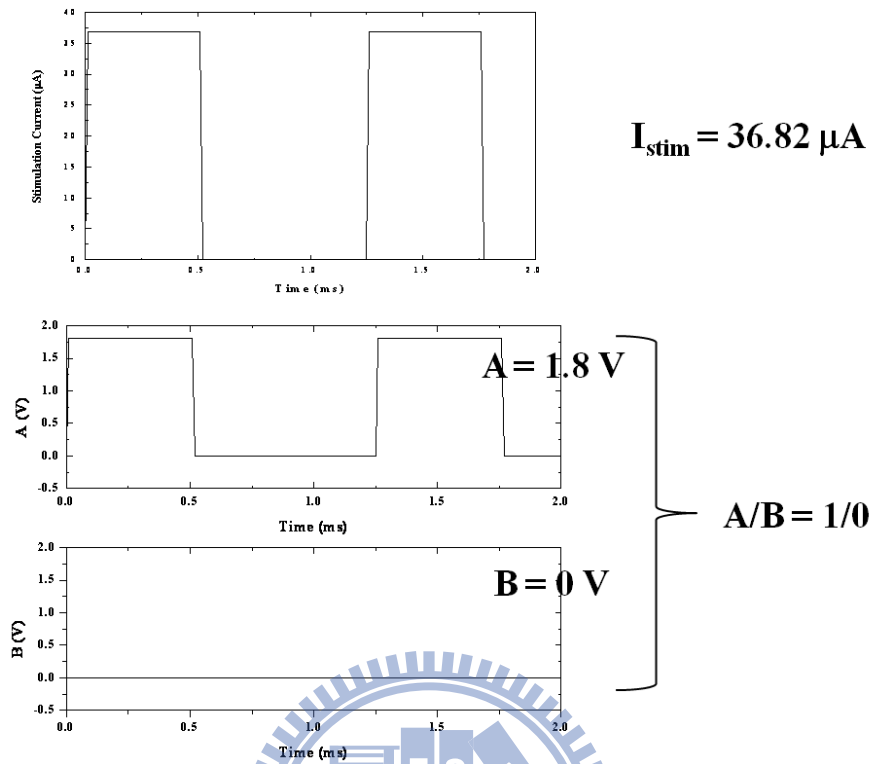


Fig. 3.18. The simulation results of stimulus current and control signals as loading impedance $R_L = 250 \text{ k}\Omega$ and operating voltage $V_{cc} = 9.36 \text{ V}$.

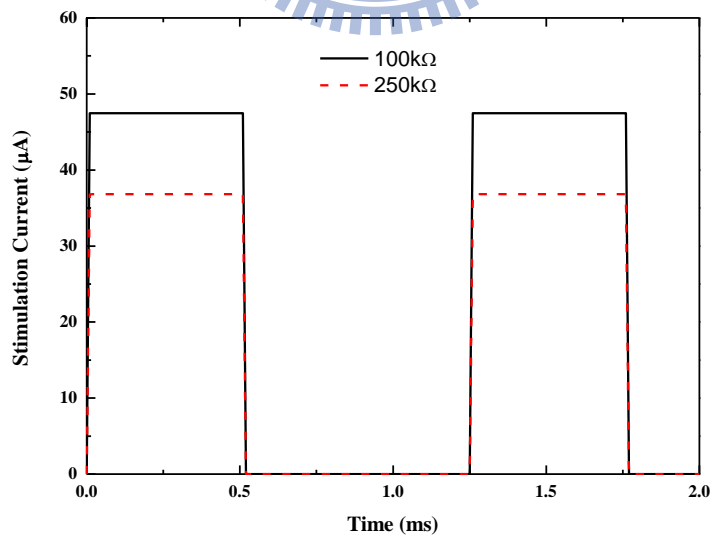


Fig. 3.19. Simulation results of stimulus current as loading impedance $R_L = 100 \text{ k}\Omega$ and $250 \text{ k}\Omega$ with their corresponding V_{cc} .

In this work, tissue impedance is classified into 4 groups as 100 k Ω ~ 130 k Ω , 130 k Ω ~ 170 k Ω , 170 k Ω ~ 210 k Ω , and 210 k Ω ~ 250 k Ω . To satisfy the proposed current range, each group of tissue impedance is designed to provide operating voltage $V_{cc} = 5.04$ V, 6.48 V, 7.92 V, and 9.36 V, respectively. The simulation results of stimulus current, operating voltage V_{cc} , and power consumption as loading impedance changing from $R_L = 100$ k Ω to $R_L = 250$ k Ω are shown in Fig. 3.20, Fig. 3.21, and Fig. 3.22, respectively. It is obvious that simulation result of power consumption looks like a four-level steps because the four different levels of V_{cc} are in use.

The proposed high-voltage-tolerant stimulus driver to suppress epileptic seizure with adaptive loading consideration has been fabricated in TSMC 0.18- μ m 1.8-V/3.3-V CMOS process. Fig. 3.23 shows the layout and chip photo of the proposed stimulus driver. The chip size of the stimulus driver is $500 \times 340 \mu\text{m}^2$.

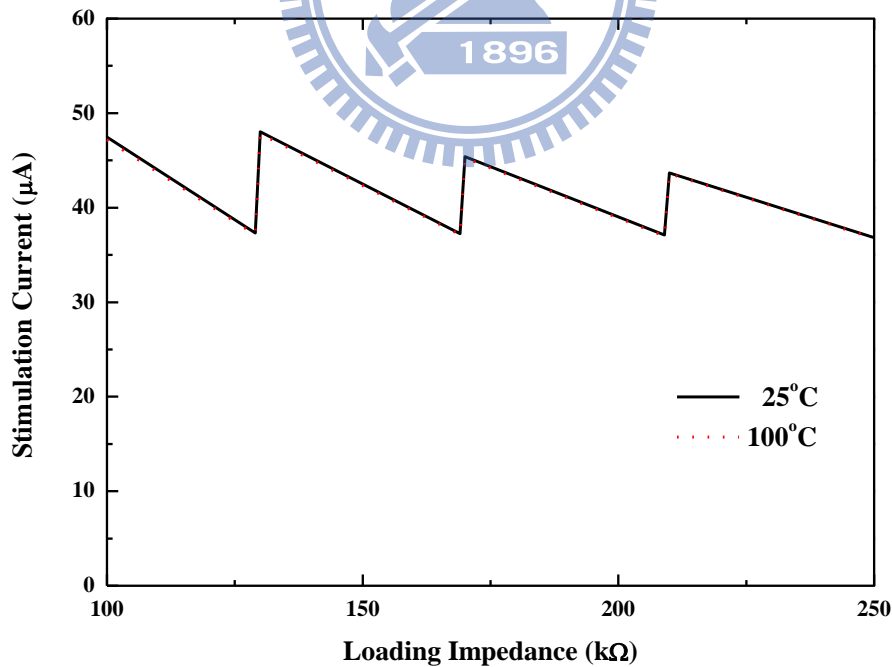


Fig. 3.20. Simulation results of stimulus current as loading impedance varying from 100 k Ω to 250 k Ω .

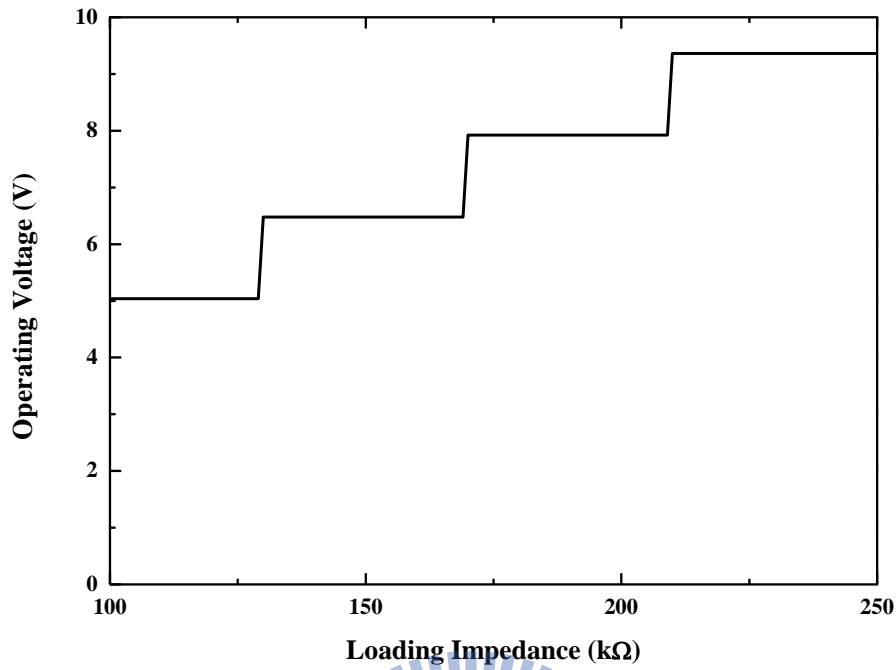


Fig. 3.21. Simulation results of operating voltage as loading impedance varying from 100 kΩ to 250 kΩ.

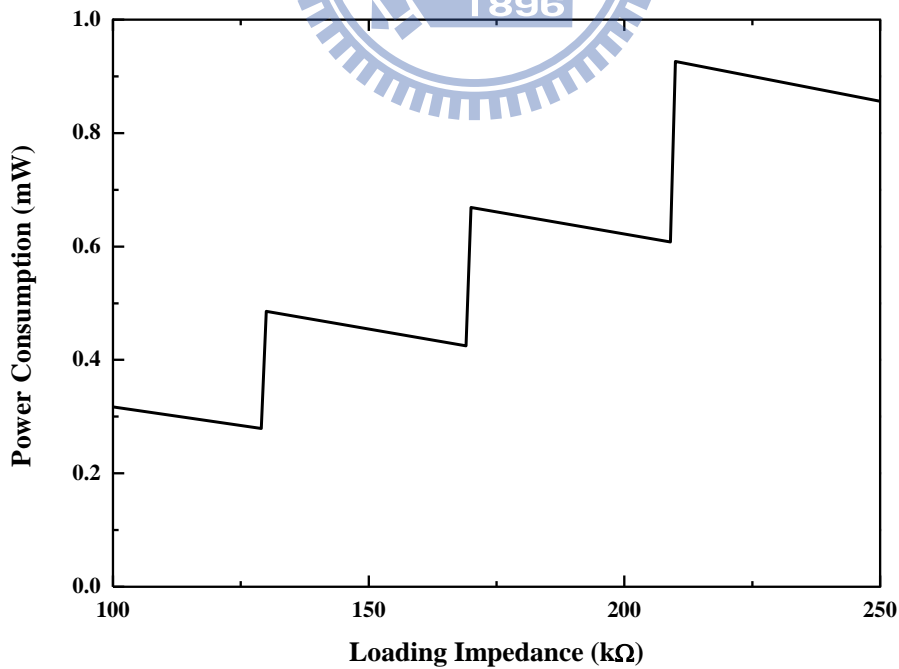
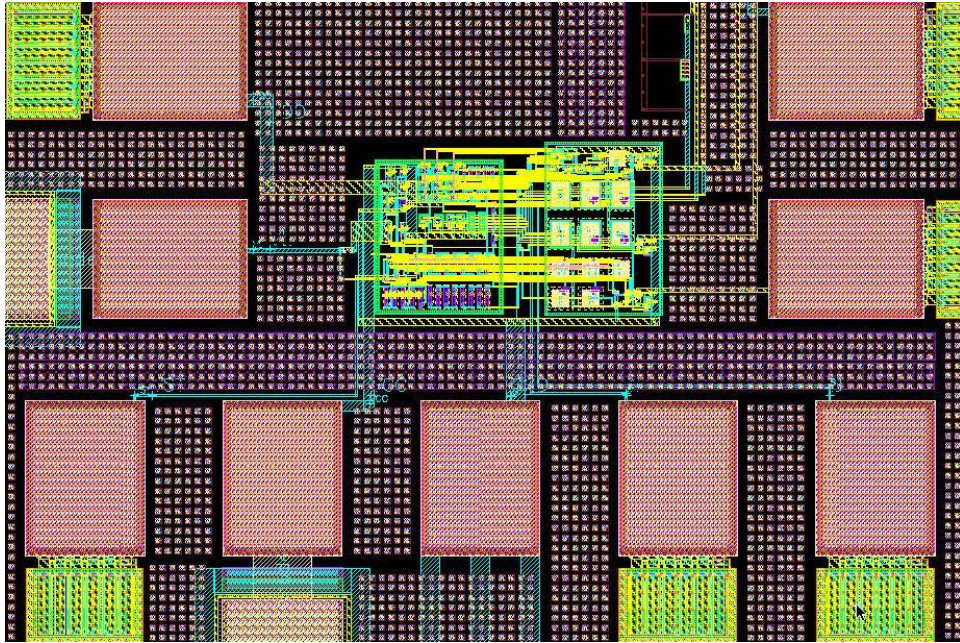
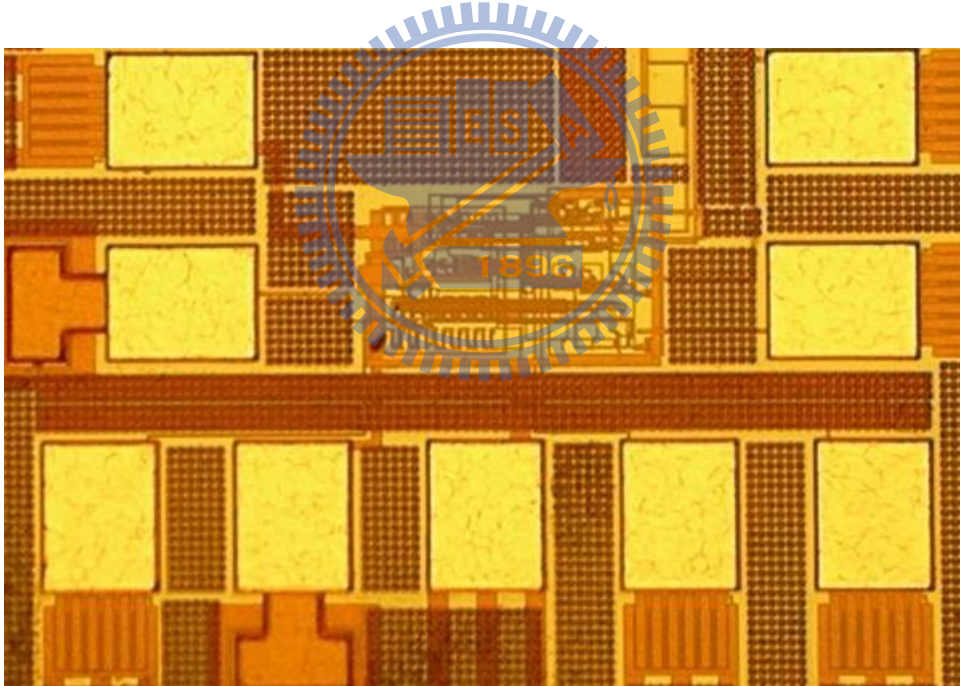


Fig. 3.22. Simulation results of power consumption as loading impedance varying from 100 kΩ to 250 kΩ.



(a)



(b)

Fig. 3.23. (a) Layout and (b) chip photo of the proposed stimulus driver.

3.2.3 Measurement Results

The measurement setup of proposed design is shown in Fig. 3.24, where two Keithley 2400 source meters, one Hp 33120A function generator, and one TDS 3054B

oscilloscope are in use. One Keithley 2400 is utilized to provide the prototype of proposed design with system supply voltage (V_{DD}) of 1.8 V, and the other is utilized to replace the charge pump system to provide variable operating voltage V_{CC} according to observed control signals A/B. Hp 33120A is utilized to provide the stimulation signal (V_{ST}) to enable stimulus driver. TDS 3054B is used to observe output voltage of the stimulus driver and control signals A/B. By dividing the output voltage by the loading impedance, the magnitude of stimulus current can be obtained.

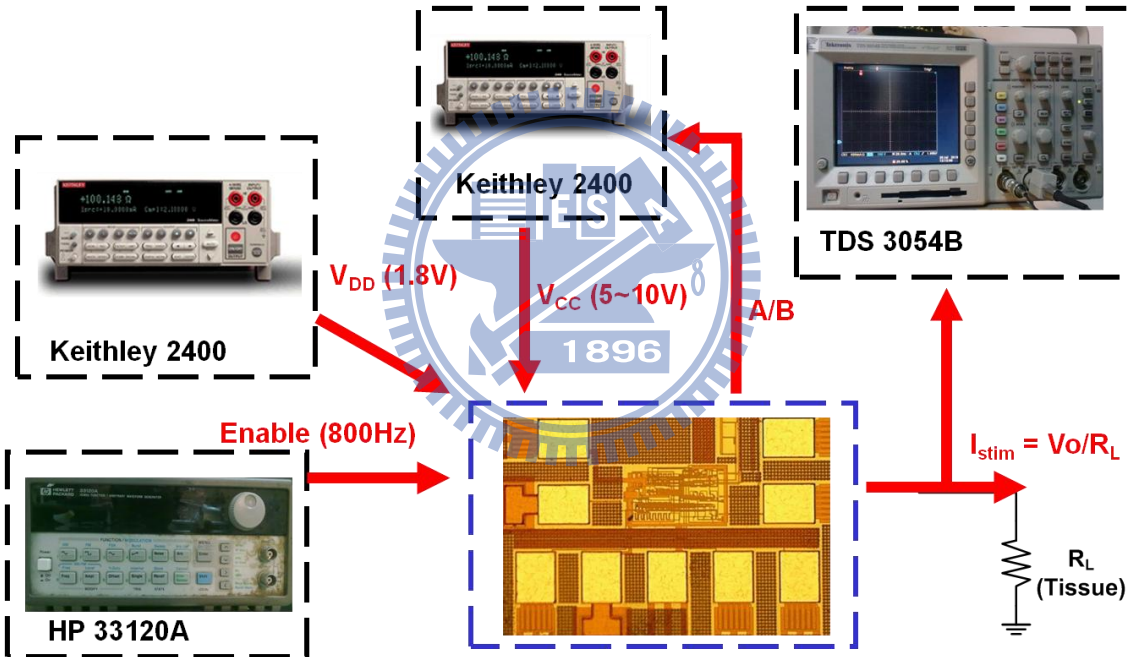


Fig. 3.24. Measurement setup of this work. Two Keithley 2400 source meters are used to provide system supply voltage (V_{DD}) and operating voltage (V_{CC}). HP 33120A function generator is utilized to provide the stimulation signal (V_{ST}). TDS 3054B is used to observe output voltage of the stimulus driver and control signals A and B.

To verify the performance of proposed stimulus driver, the process which we use to decide the correct V_{CC} with corresponding R_L while doing simulation is taken. Also, the upper limit tissue impedance of this design ($R_L = 250 \text{ k}\Omega$) is adopted. At the beginning,

V_{cc} is set to be 5.04 V originally, the observed stimulus current $I_{stim} = 19.2 \mu A$, and control signals $A/B = 0/1$ as shown in Fig. 3.25. With corresponding to $A/B = 0/1$, V_{cc} should be set to 6.48 V, and then repeat the measurement. The measurement results for $V_{cc} = 6.48$ V are $I_{stim} = 24.96 \mu A$, and control signals $A/B = 1/1$ as shown in Fig. 3.26. With corresponding to $A/B = 1/1$, V_{cc} should be change to 7.92 V, and then repeat the measurement. The measurement results for $V_{cc} = 7.92$ V are $I_{stim} = 31.36 \mu A$, and control signals $A/B = 1/0$ as shown in Fig. 3.27. Measurement should be repeat again with $V_{cc} = 9.36$ V since $A/B = 1/0$. The measurement results for $V_{cc} = 9.36$ V are $I_{stim} = 37.2 \mu A$, and control signals $A/B = 1/0$ as shown in Fig. 3.28. According to the above measurement procedure, the function to generate correct control signals A and B is verified. The measurements results as loading impedance $R_L = 100$ k Ω and 250 k Ω with their corresponding V_{cc} are shown in Fig. 3.29.

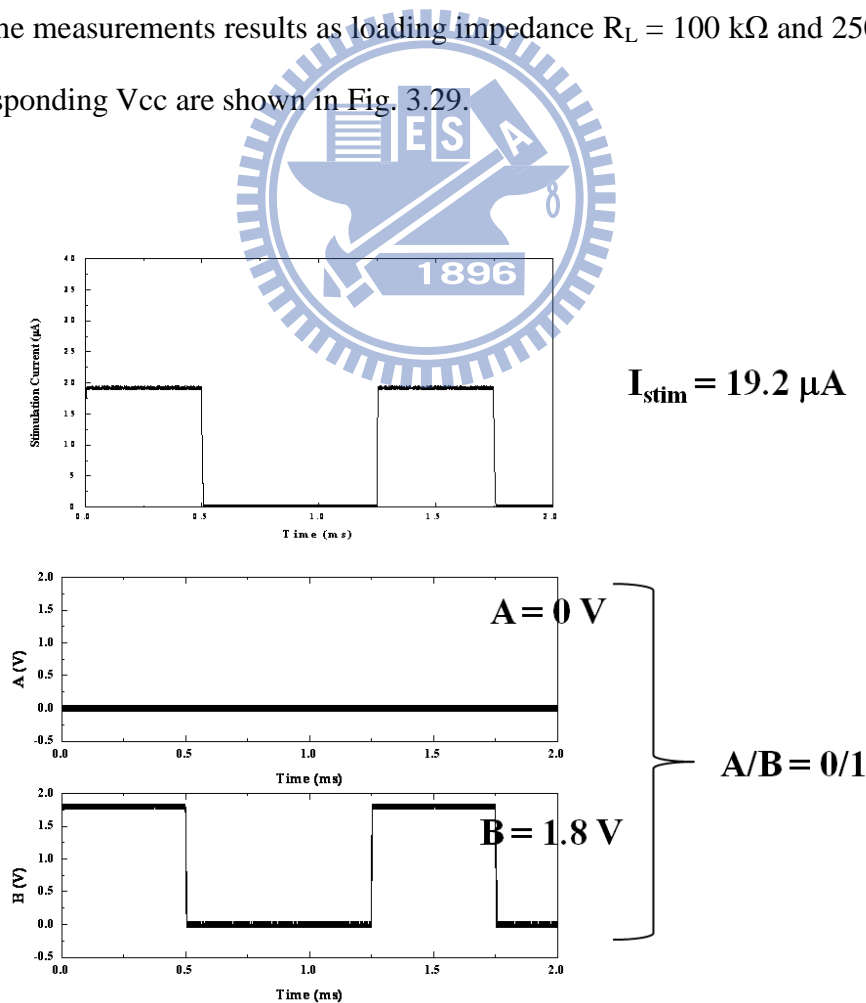


Fig. 3.25. The measurement results of stimulus current and control signals as loading impedance $R_L = 250$ k Ω and operating voltage $V_{cc} = 5.04$ V.

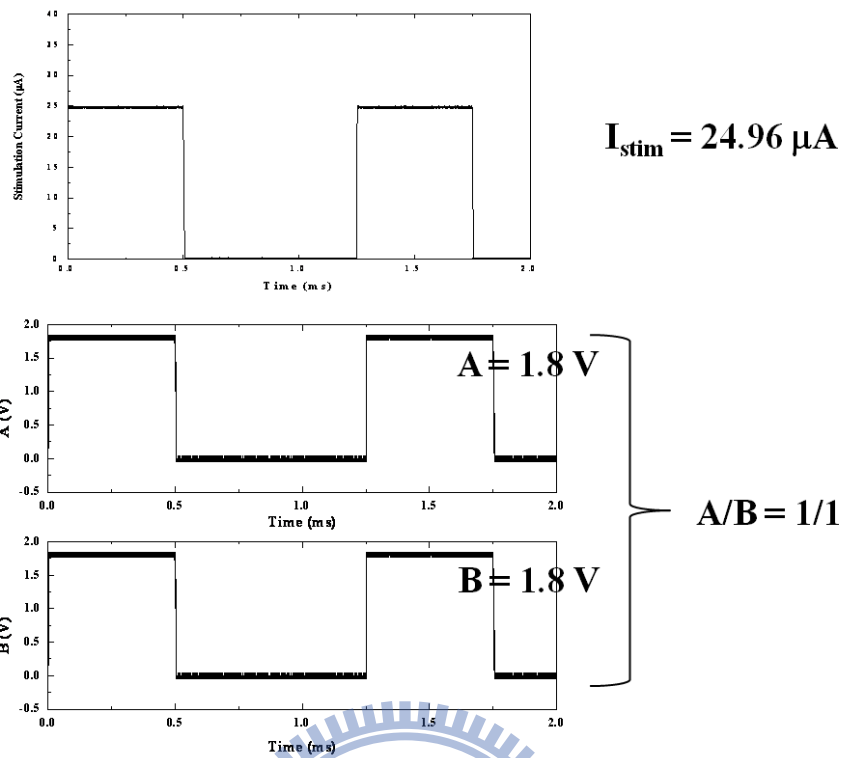


Fig. 3.26. The measurement results of stimulus current and control signals as loading impedance $R_L = 250 \text{ k}\Omega$ and operating voltage $V_{cc} = 6.48 \text{ V}$.

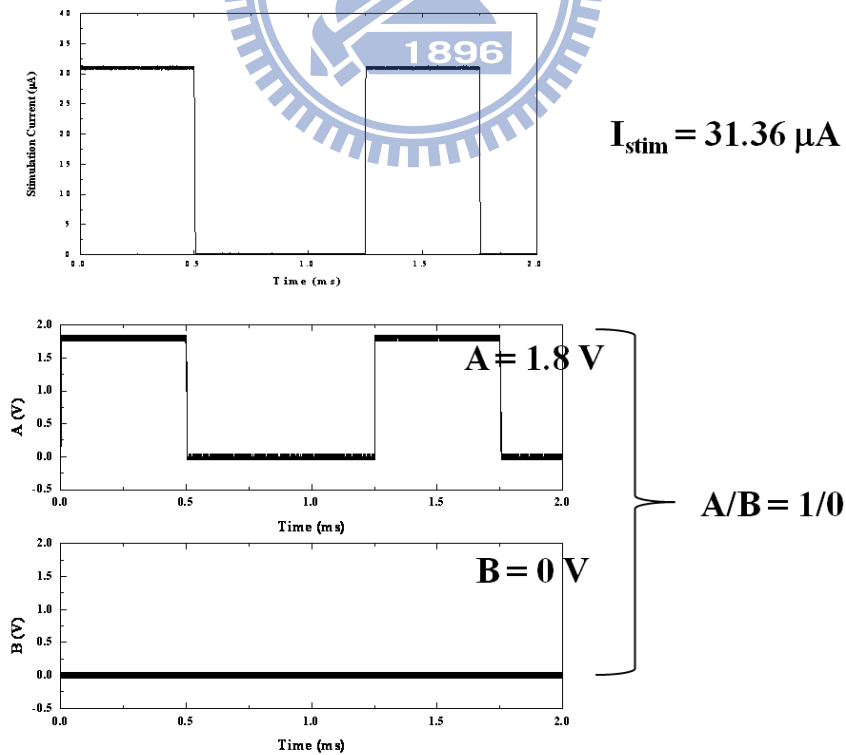


Fig. 3.27. The measurement results of stimulus current and control signals as loading impedance $R_L = 250 \text{ k}\Omega$ and operating voltage $V_{cc} = 7.92 \text{ V}$.

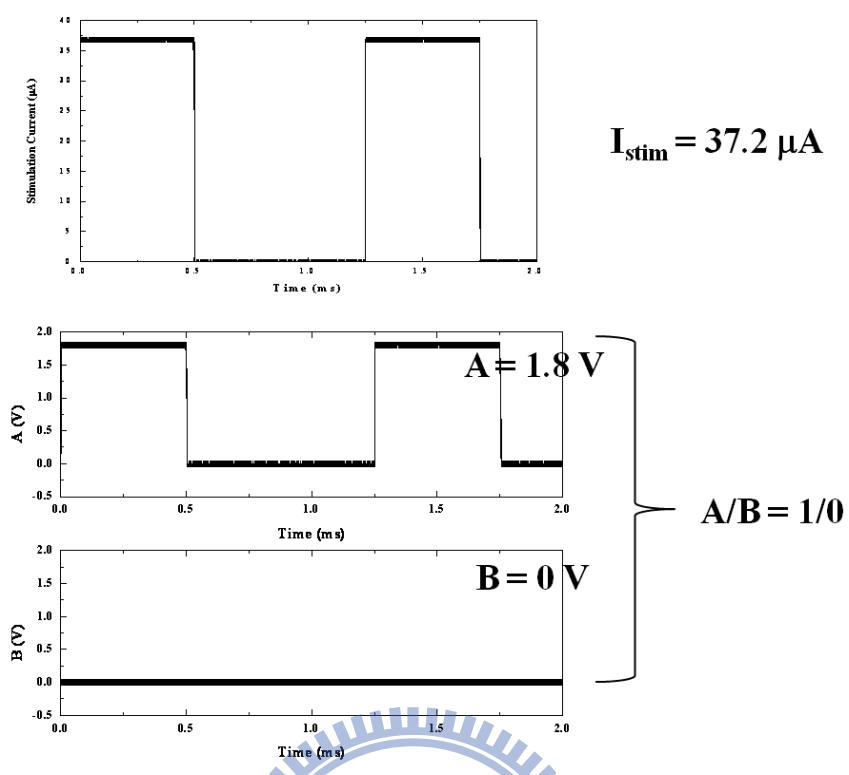


Fig. 3.28. The measurement results of stimulus current and control signals as loading impedance $R_L = 250 \text{ k}\Omega$ and operating voltage $V_{cc} = 9.36 \text{ V}$.

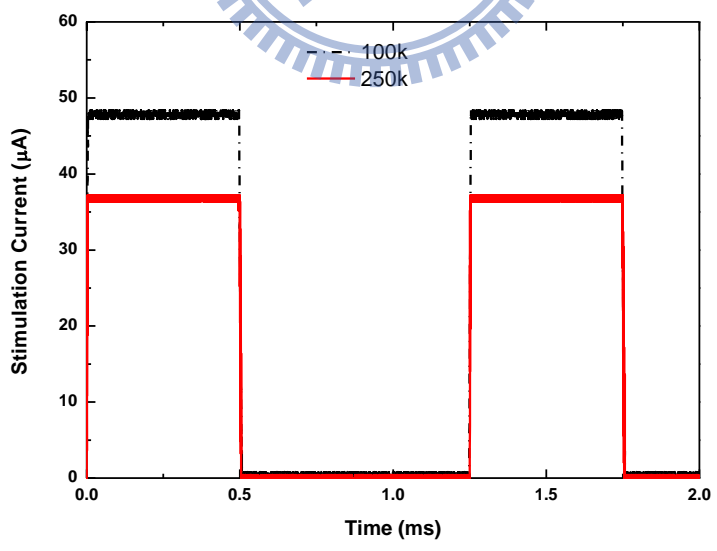


Fig. 3.29. Measurement results of stimulus current as loading impedance $R_L = 100 \text{ k}\Omega$ and $250 \text{ k}\Omega$ with their corresponding V_{cc} .

Fig. 3.30 shows the measurement result of stimulus current as loading impedance changing from $R_L = 100 \text{ k}\Omega$ to $R_L = 250 \text{ k}\Omega$. The measurement result shows that loading impedance is classified into 4 groups as $100 \text{ k}\Omega \sim 133 \text{ k}\Omega$, $133 \text{ k}\Omega \sim 168 \text{ k}\Omega$, $168 \text{ k}\Omega \sim 213 \text{ k}\Omega$, and $213 \text{ k}\Omega \sim 250 \text{ k}\Omega$. The result is close to our design which we classify loading impedance into 4 groups as $100 \text{ k}\Omega \sim 130 \text{ k}\Omega$, $130 \text{ k}\Omega \sim 170 \text{ k}\Omega$, $170 \text{ k}\Omega \sim 210 \text{ k}\Omega$, and $210 \text{ k}\Omega \sim 250 \text{ k}\Omega$ originally. The stimulus current is in the range of $36.98 \mu\text{A} \sim 49.6 \mu\text{A}$, which fits in the range of $35 \mu\text{A} \sim 50 \mu\text{A}$. The measurement results of operating V_{cc} and power consumption are shown in Fig. 3.31 and Fig. 3.32. The power consumption is within 0.24 mW to 0.87 mW .

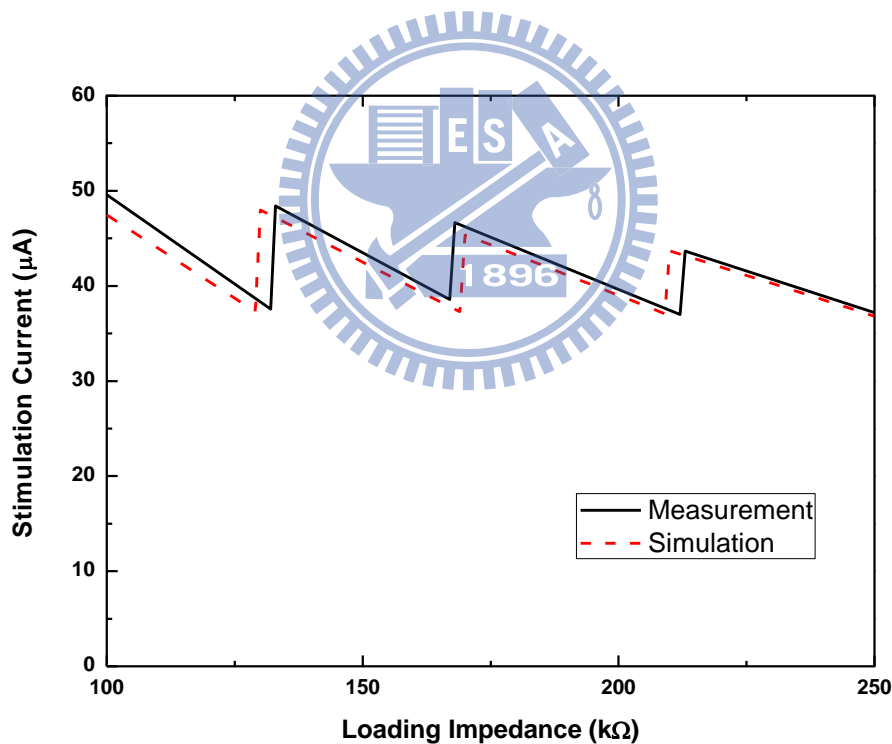


Fig. 3.30. Measurement results of stimulus current as loading impedance varying from $100 \text{ k}\Omega$ to $250 \text{ k}\Omega$.

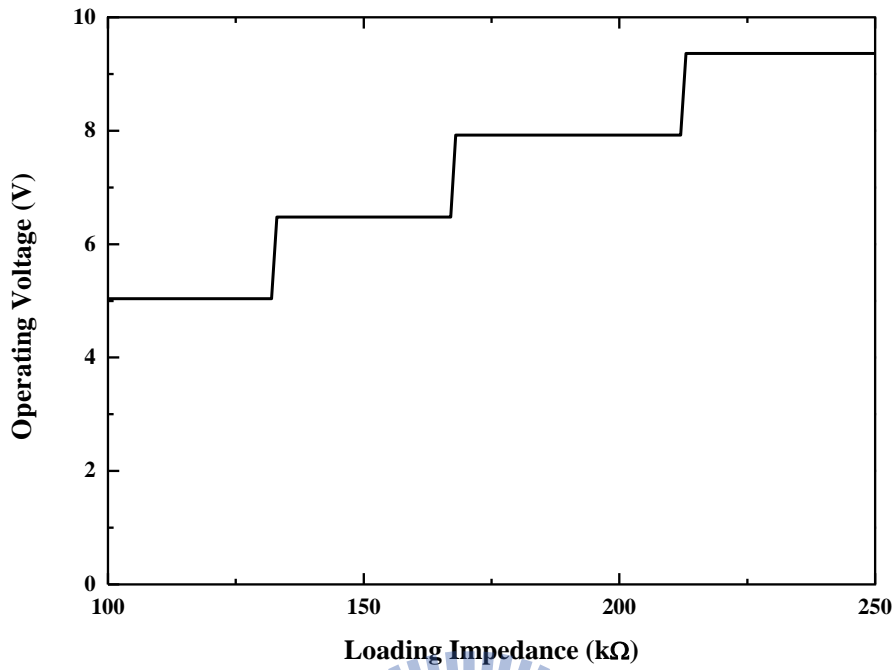


Fig. 3.31. Measurement results of operating voltage as loading impedance varying from 100 kΩ to 250 kΩ.

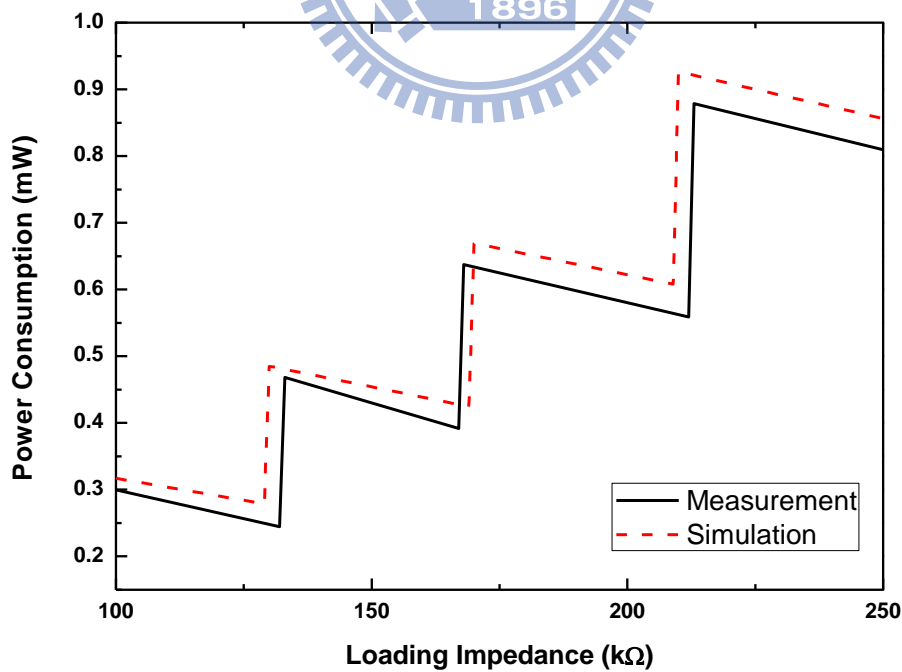


Fig. 3.32. Measurement results of power consumption as loading impedance varying from 100 kΩ to 250 kΩ.

3.2.4 Integration of the Proposed Stimulus Driver and Epileptic Seizure Monitoring and Controlling System

The animal test experiment is conducted by Neural Computing and Brain Computer Interface Lab of National Cheng-Kung University. In this experiment, the stimulus driver has been integrated into the closed-loop epileptic seizure monitoring and controlling system. Long-evans rats, born with spontaneous absence epileptic seizure, are selected for experiment in this study. The rats of aged 4 - 6 months and weighting 500 - 700 g were anesthetized with sodium pentobarbital (50 mg/kg, i.p.). All surgical and experimental procedures were reviewed and approved by Institutional Animal Care and Use Committee of National Cheng-Kung University.

The closed-loop epileptic seizure monitoring and controlling system consists of data acquisition (EEG detection), wireless transceiver, host computer (signal process), microcontroller (stimulator activation). By analyzing brain activities of Long-evans rats which suffer from spontaneous absence seizure and epileptiform activities induced by pentylenetetrazol (PTZ), the system can detects epileptic seizure simultaneously and stimulates the right-side zona incerta (ZI) (posterior 4.0 mm, lateral 2.5 mm, and depth 6.7-7.2 mm). Stimulus current is conducted by a 4-microwire bundle, each made of Teflon-insulted stainless steel wire while ground electrode was implanted 2 mm caudal to lambda.

Fig. 3.33 shows the measurement setup of integration experiment of proposed stimulus driver and closed-loop epileptic seizure monitoring and controlling system. An additional computer is used to receive and process the EEG signals to decide whether epileptic seizure happens or not, and then sends the control signals back. The chips utilized to detect brain activities of Long-evans rats, send EEG signals to the computer, and receive control signals from the computer to activate the stimulus driver on the rat's head are shown in Fig. 3.34.

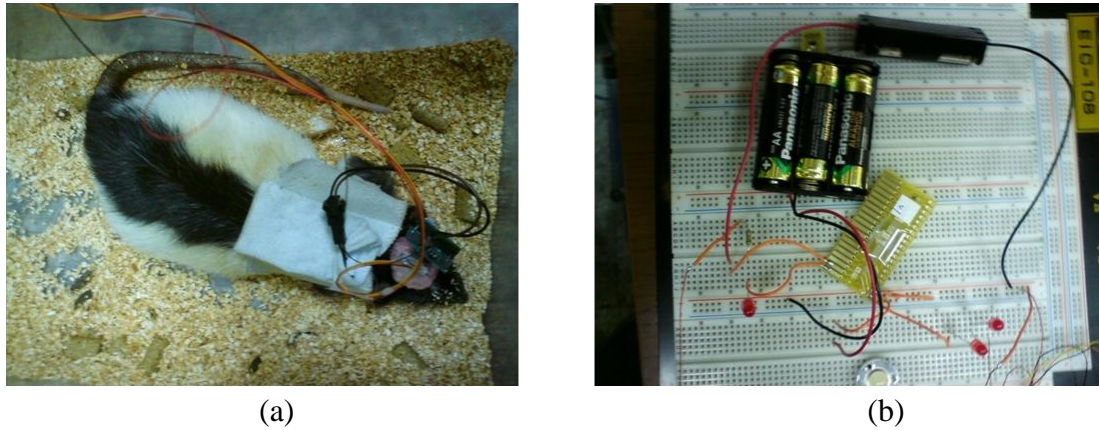


Fig. 3.33. Measurement setup of integration experiment of proposed stimulus driver and closed-loop epileptic seizure monitoring and controlling system. (a) Long-evans rats in this experiment, and (b) the proposed stimulus driver.

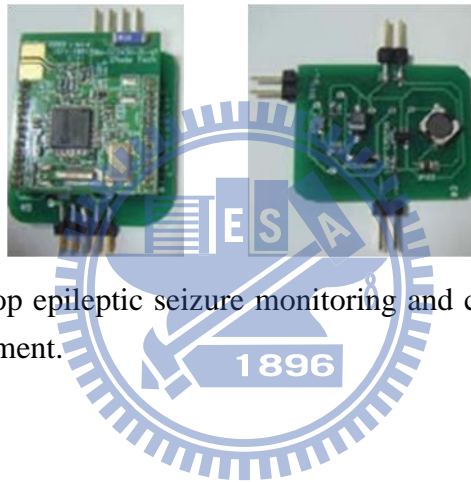


Fig. 3.34. The closed-loop epileptic seizure monitoring and controlling system utilized in this animal test experiment.

Before integrating stimulus driver into the closed-loop system, we observe the brain activities of the rat and provide stimulus current manually by Grass S48 Square Pulse Stimulator to suppress epileptic seizure and obtain the equivalent loading impedance of the brain tissue of the rat. The effective stimulus current for the rat in this experiment is $20 \mu\text{A}$, and output voltage $\sim 4.8 \text{ V}$ is observed at the output node of the machine. The equivalent loading impedance can be derived from Eq. (3-4).

$$4.8 \text{ V} / 20 \mu\text{A} = 240 \text{ k}\Omega \quad (3-4)$$

By experience of animal experiment, stimulus current with 800 Hz and 40 % duty cycle

is efficient to regulate the abnormal discharge. Whenever epileptic seizure monitoring and controlling system detects epileptiform activity, stimulus driver delivers the specified current that mentioned above for 0.5 second. To avoid the 60Hz noise, we don't use any machine including power supply and function generator in the formal experiment. V_{DD} is supplied by one 1.6-V battery and V_{CC} is supplied by three 1.6-V batteries. The stimulation signal (V_{ST}) of 800 Hz and 40 % duty cycle is generated by the closed-loop controlling system. Whenever the system detects epileptic seizure, the proposed stimulus driver is given a stimulation signal and stimulates ZI. Duration of stimulation is 0.5 s. Fig. 3.35 shows the stimulation wave at the output of stimulus driver.

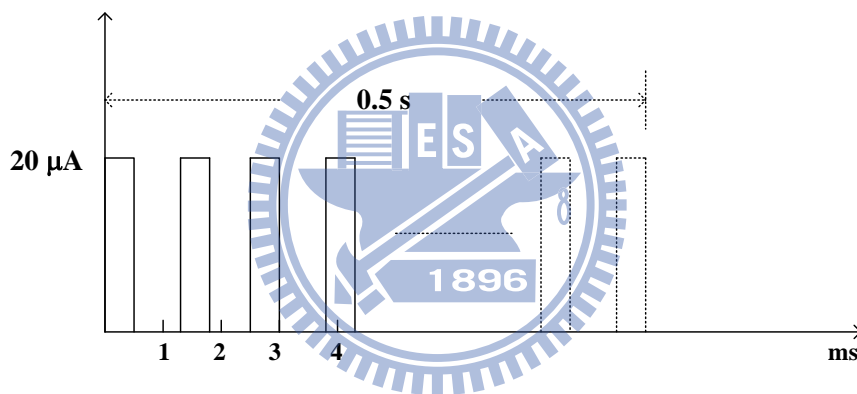
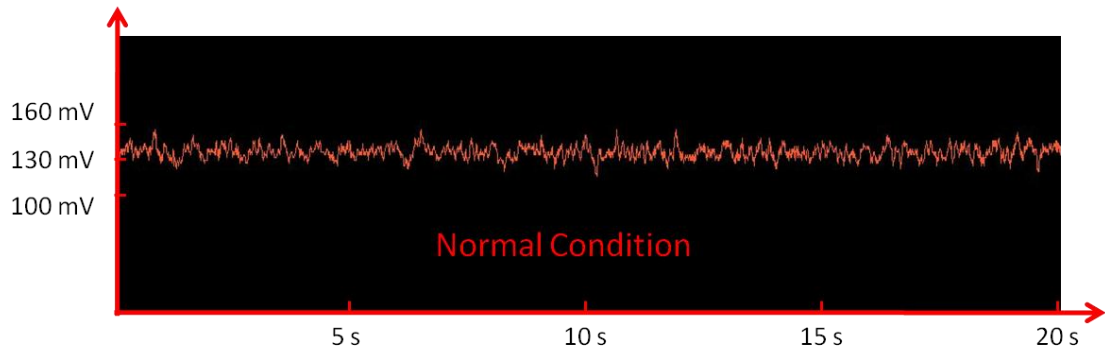
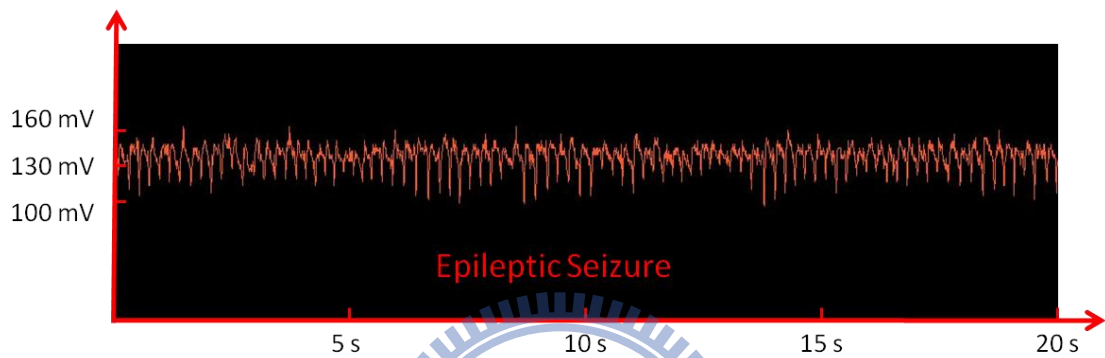


Fig. 3.35. The waveform of stimulus current provided by the proposed stimulus driver in this animal test experiment.

The brain activities (EEG) are detected and then recorded by the computer. The EEG of the rat under normal condition is shown in Fig. 3.36(a). During epileptic seizure time, the waveform of lower frequency and higher magnitude is recorded as shown in Fig. 3.36(b). Fig. 3.37 shows the process of epileptic seizure, stimulation, and seizure suppression. At about $t = 10$ s, epileptiform activity is detected, the stimulation signal is generated immediately and the stimulus driver delivers stimulus current to the rat. After few seconds, the epileptic seizure is suppressed and the EEG recovers.



(a)



(b)

Fig. 3.36. The EEG of the Long-Evans rat under (a) normal condition and (b) epileptic seizure in this animal test experiment.

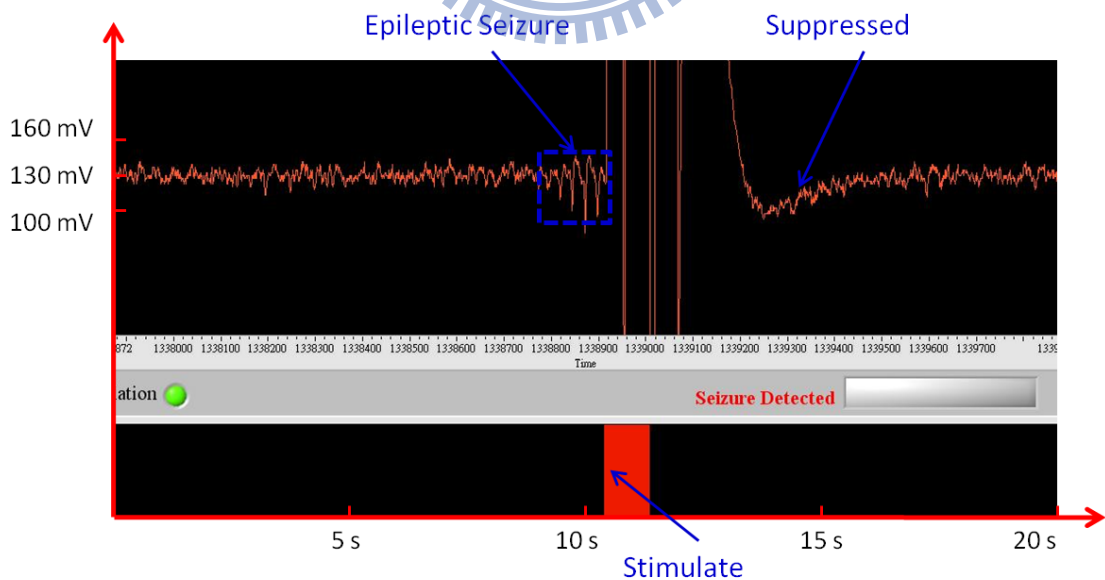
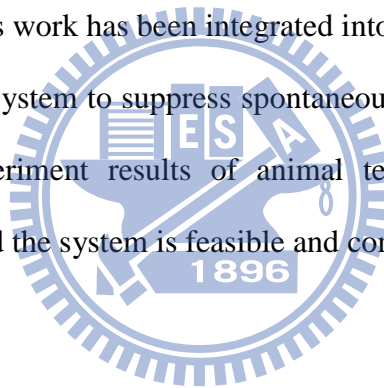


Fig. 3.37. The procedure of normal condition, epileptic seizure, stimulus driver activated, and epileptic seizure suppressed.

3.3 Summary

Design of high-voltage-tolerant stimulus driver to suppress epileptic seizure with adaptive loading consideration is investigated and verified in this chapter. While the loading impedance varies from 100 k Ω to 250 k Ω , the proposed stimulus driver fabricated in 0.18- μm 1.8-V/3.3-V CMOS process with stacked MOS structure can provide stable stimulus current ($\sim 40 \mu\text{A}$) and sustain the high voltage ($\sim 10 \text{V}$) without gate-oxide overstress problem. The stimulus driver classifies loading impedance into four groups and each group is provided with adjustable operating voltage V_{cc} . In comparison with conventional works with fixed operating voltage, this work consumes less power. Furthermore, this work has been integrated into closed-loop epileptic seizure monitoring and controlling system to suppress spontaneous absence epileptic seizure of Long-evans rats. The experiment results of animal test show that integration of proposed stimulus driver and the system is feasible and compatible.



Chapter 4

Conclusions and Future Works

4.1 Conclusions

There are tens of millions of people in the world who suffer from epileptic seizure. Though most of the patients can make their syndromes improved by taking traditional therapies such as pharmacologic treatment and surgical treatment. For those patients who are drug-resistant and high-risk surgical, electrical stimulation treatment is also an alternative. Electrical stimulation treatment is an innovative therapy combining electronics technology and medical science. The therapeutic device is consisted of interface between electrical device and human body, signal processing, and stimulus driver. Through the interface, stimulus driver provides stimulus current into brain of human to suppress epileptic seizure. Vagus nerve stimulation (VNS), an electrical stimulation treatment which has been approved, is a successful example. In recent years, using implantable devices to provide electrical stimulation treatment has been investigated. This work investigates the output stage of the therapeutic device, stimulus driver.

To be integrated into SoC with other parts of the implantable epileptic prosthetic, this work has been fabricated in TSMC 0.18- μm 1.8-V/3.3-V CMOS process. The stimulus driver consists of the high-voltage-tolerant output driver, and V_{CC} control circuit. The stacked MOS configuration with 3.3-V transistors is adopted in output driver to sustain the circumstance of high operating voltage without gate-oxide overstress, thus enhance reliability. By using stacked MOS configuration, the output

resistance of output driver is large and hence this work has large voltage compliance. With adaptive loading consideration, voltage-mode feedback control is utilized and implemented by Vcc control circuit in this work. Loading impedance is classified into four groups, and each group is provided by the corresponding operating voltage. By using adjustable operating voltage, this proposed stimulus driver is more power efficient than those previous works with fixed operating voltage. According to measurement results, stimulus current is within 35 μA to 50 μA which is one of the purpose of this work, and power consumption is in the range of 0.24 mW ~ 0.87 mW as loading impedance varies from 100 k Ω to 250 k Ω . This proposed stimulus driver has been integrated into closed-loop epileptic seizure monitoring and controlling systems, and an animal test experiment to verify the performance is conducted by Neural Computing and Brain Computer Interface Lab of National Cheng-Kung University. According to the experimental results, spontaneous absence seizures of Long-Evans rats can be successfully suppressed by the stimulus current provided by the work.

Table 4.1 summarizes the proposed stimulus driver.

Table 4.1. Summary of the proposed stimulus driver.

Technology	0.18-μm 1.8-V/3.3-V CMOS Process
Layout Area	500 μm x 340 μm
Adaptable Tissue Impedance	100 kΩ – 250 kΩ
Stimulus Current	36.98 μA – 49.6 μA
Supply VDD	1.8 V
Adaptive Control	5.04V for $R_L= 100\text{k}\Omega \sim 132\text{k}\Omega$ 6.48V for $R_L= 133\text{k}\Omega \sim 167\text{k}\Omega$ 7.92V for $R_L= 168\text{k}\Omega \sim 212\text{k}\Omega$ 9.36V for $R_L= 213\text{k}\Omega \sim 250\text{k}\Omega$
Power Consumption	0.24 mW – 0.87 mW

4.2 Future Works

4.2.1 Integration with Charge Pump System

In this work, operating voltage V_{cc} is provided by a power supply with corresponding control signals A/B. However, the use of power supply is not allowed while implanting the epileptic prosthetic into a patient's body. Thus an additional charge pump which is used to generate high operating voltage (~ 10 V) should be integrated with output driver and V_{cc} control circuit to complete the whole stimulus driver system as shown in Fig. 4.1. After combining charge pump system, some issues such as power consumption the relationship between rise time of charge pump and stimulus current should be investigated.

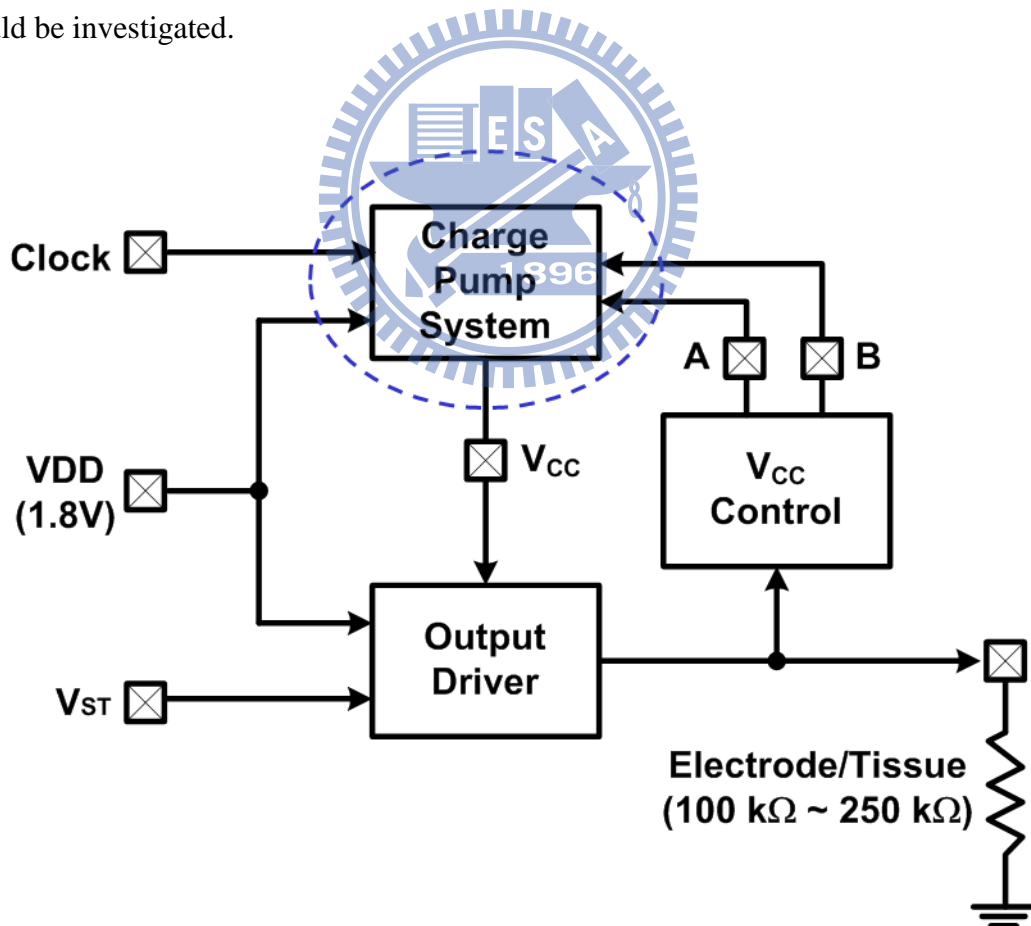


Fig. 4.1. Stimulus driver integrated with charge pump system.

4.2.2 An Additional Slew-rate Clamping Circuit Should Be Added

Fig. 4.2 shows the waveform of voltage observed at the electrode while stimulating the rat's brain tissue with fixed stimulus current of 20 μA (800 Hz, duty cycle = 40%). Fig. 4.3 shows the voltage drop across a resistor (200 k Ω) while current of 20 μA flowing through it. To compare Fig. 4.2 with Fig. 4.3, we notice that the slope of the waveform in Fig. 4.2 is less than that in Fig. 4.3, so there may be a parasitic capacitor in the equivalent model of brain tissue. If the slew rate of output voltage of stimulus driver is large, the transient current at the beginning of stimulation period may be too large according to Eq. (4-1).

$$i = C \times dV/dt \quad (4-1)$$

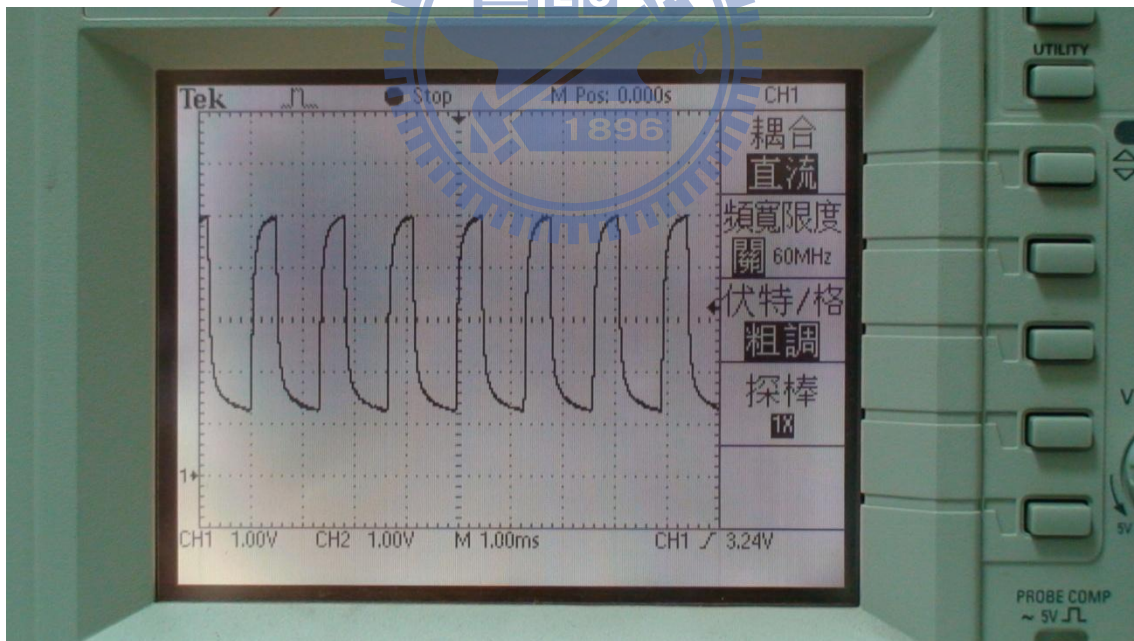


Fig. 4.2. The waveform of voltage observed at the electrode while stimulating the rat's brain tissue with fixed stimulus current of 20 μA (800 Hz, duty cycle = 40%).

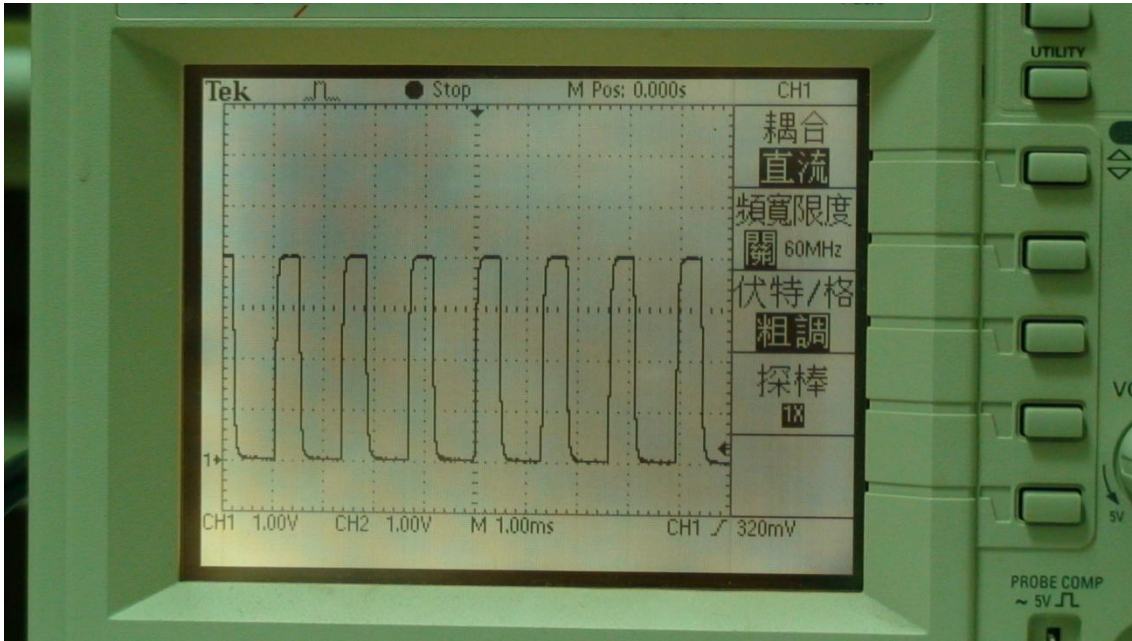


Fig. 4.3. The waveform of voltage drop across a resistor (200 k Ω) while stimulus current of 20 μ A (800 Hz, duty cycle = 40%) flowing through it.

Hence an additional clamping circuit should be added to this proposed stimulus driver to limit the slew rate of output voltage. From Fig. 4.2, we can derive the max slew rate as shown in Eq. (4-2).

$$\text{Max slew rate} \cong 3\text{V}/0.1\text{ms} = 30,000 \text{ V/s} \quad (4-2)$$

4.2.3 Design of Bi-Phase Stimulus Driver

Some studies revealed that unbalanced stimulus current may cause net charge to store in body and lead to destructive problems such as electrolysis, gazing, pH changing, and dissolution [31], [32]. In order to solve these problems, the design of bi-phase stimulus driver is required. There are two ways to transfer biphasic stimulus current. The first way is to use both positive and negative power supplies with one electrode per stimulus site as shown in Fig. 4.4. The second way is to use only positive power supply

with two electrodes per stimulus site as shown in Fig. 4.5.

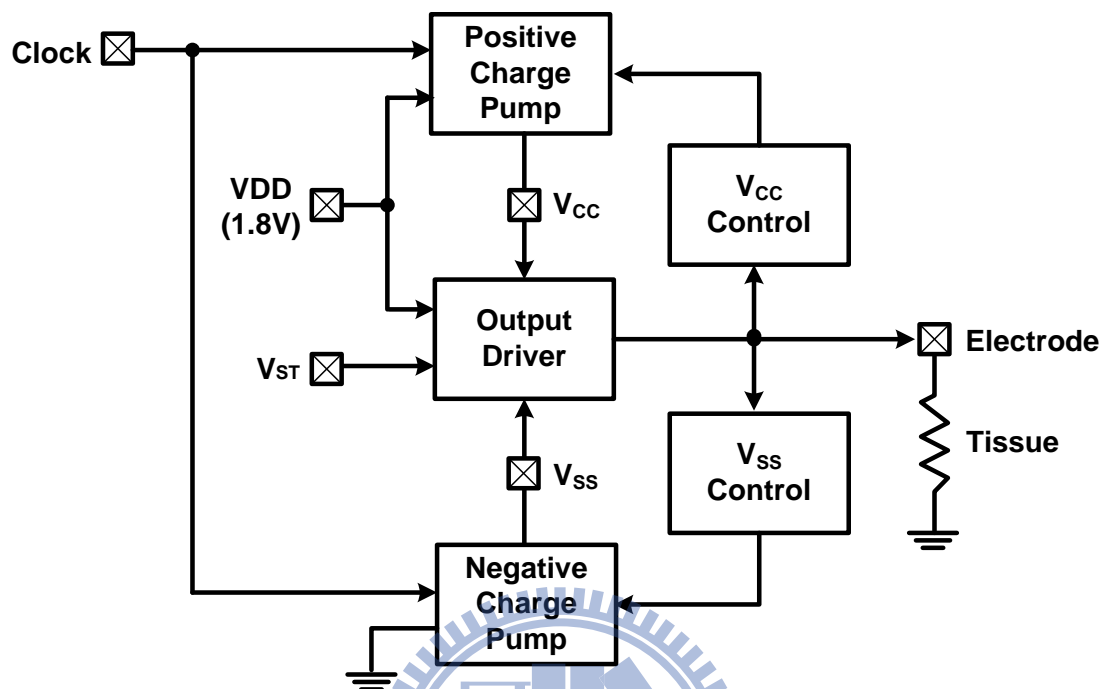


Fig. 4.4. Bi-phase stimulus driver with both positive and negative powers provides biphasic stimulus current through one electrode per stimulus site.

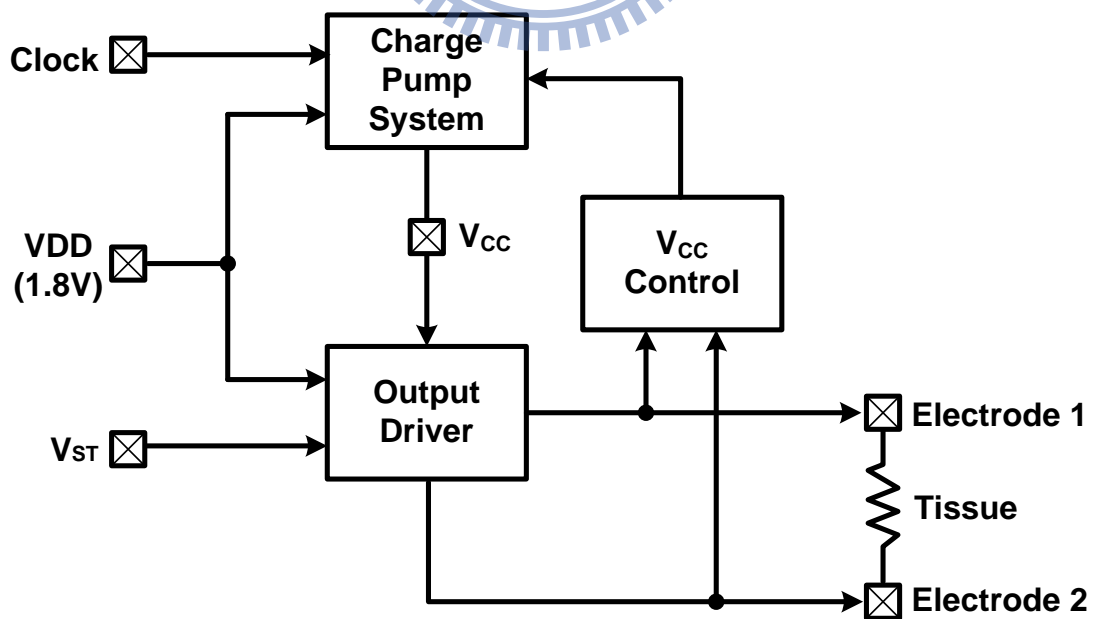


Fig. 4.5. Bi-phase stimulus driver with only positive power provides biphasic current between two electrodes per stimulus site.

Using the second method to achieve the purpose of delivering biphasic stimulus current, we can just copy the output driver of this proposed stimulus driver and place it symmetrically to the original one as shown in fig. 4.6. An extra control signal is also required to achieve charge balance during the stimulation period.

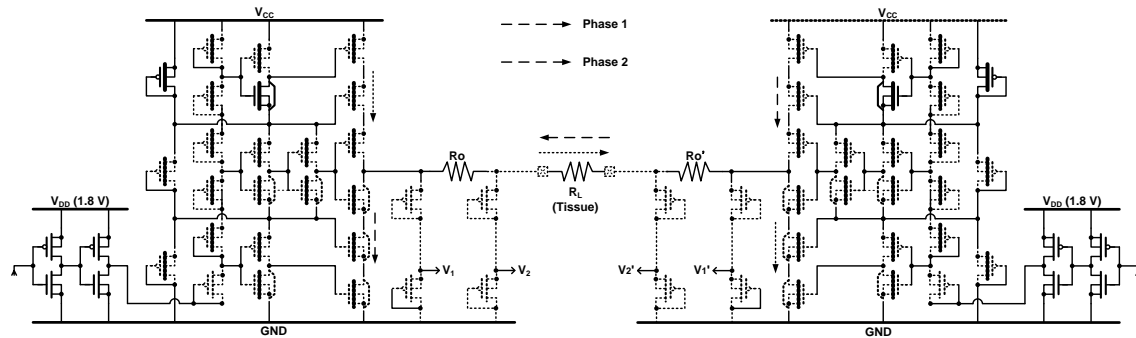
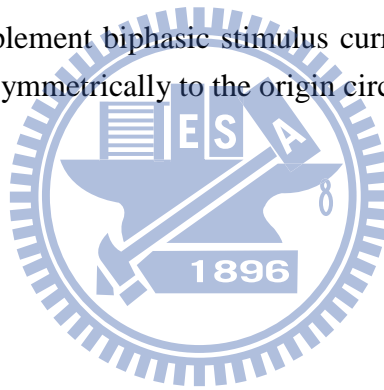


Fig. 4.6. The method to implement biphasic stimulus current by making a copy of the output driver and placing it symmetrically to the origin circuit.



References

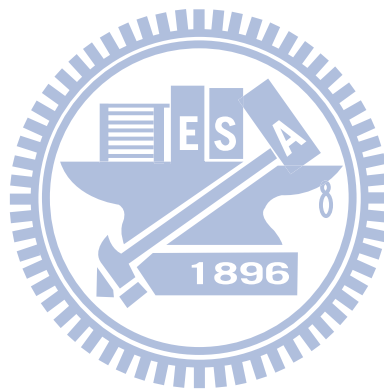
- [1] S. Cantor and S. Cantor, "Physiological description of the neuron and the human nervous system," in *Proc. IEEE Int. Frequency Control Symp.*, 1995, pp. 3-9.
- [2] M. Sivaprakasam, W. Liu, J. Weiland, and M. Humayun, "A variable range bi-phasic current stimulus driver circuitry for an implantable retinal prosthetic device," *IEEE J. Solid-State Circuits*, vol. 40, no. 3, pp. 763-771, Mar. 2005.
- [3] L. Zhao, W. Wu, Z. Liang, and G. Hu, "Nonlinear analysis in treatment of intractable epilepsy with EEG biofeedback," in *Proc. Int. IEEE EMBS Conf.*, 2005, pp. 4568-4571.
- [4] H. Gui, Y. Xia, F. Liu, X. Liu, S. Dai, L. Lei, and Y. Wang, "Based on the time-frequency analysis to distinguish different epileptiform EEG signals," in *Proc. ICBBE Bioinformatics and Biomedical Engineering Conf.*, 2009, pp. 1-4.
- [5] W. Stacey and B. Litt, "Technology insight: neuroengineering and epilepsy - designing devices for seizure control," *Nature Clinical Practice Neurology*, vol. 4, pp. 190-201, Feb. 2008.
- [6] I. Chen, J. Choi, and C. Hu, "The effect of hot-carrier stressing on gate-oxide integrity in MOSFETs," *IEEE Trans. Electron Devices*, vol. 35, no. 12, pp. 2253-2258, Dec. 1988.
- [7] R. Scott, N. Dumin, T. Hughes, D. Dumin, and B. Moore, "Properties of high-voltage stress generated traps in thin silicon oxide," *IEEE Trans. Electron Devices*, vol. 43, no. 7, pp. 1133-1143, Jul. 1996.
- [8] T. Furukawa, D. Turner, S. Mittl, M. Maloney, R. Serafin, W. Clark, L. Longenbach, and J. Howard, "Accelerated gate-oxide breakdown in mixed-voltage I/O buffers," in *Proc. IEEE Int. Reliability Physics Symp.*, 1997, pp. 169-173.
- [9] Nervous System Diagram. [online]. Available: http://zh.wikipedia.org/zh-tw/File:Nervous_system_diagram.png
- [10] D. Cofer, "Neuron basics," *Nature*, 2002. [online]. Available: <http://www.mindcreators.com/index.htm> [accessed: Jul. 6, 2011].
- [11] G. Loiseau, B. Duché, S. Cordova, J. Dartigues, and S. Cohadon, "Prognosis of benign childhood epilepsy with centrotemporal spikes. A follow-up of 168 patients," *Epilepsia*, vol. 29, no. 3, pp. 229-235, Jun. 1988.
- [12] R. Kuzniecky and B. Rosenblatt, "Benign occipital epilepsy: a family study," *Epilepsia*, vol. 28, no. 4, pp. 346-350, Jul. 1987.
- [13] R. D'Ambrosio and J. Miller, "What is an epileptic seizure? Unifying definition in clinical practice and animal research to develop novel treatments," *Epilepsy Curr.*, vol.10, no. 3, pp. 61-66, May. 2010.

- [14] A. Geva, "Forecasting generalized epileptic seizures from the EEG signal by wavelet analysis and dynamic unsupervised fuzzy clustering," *IEEE Trans. Biomedical Engineering*, vol. 45, no. 10, pp. 1205-1216, Oct. 1998.
- [15] G. Cascino, "Epilepsy: contemporary perspectives on evaluation and treatment," *Mayo Clinic Proc.*, vol. 69, no. 12, pp. 1199-1211, Dec. 1994.
- [16] G. Birback, R. Hays, X. Cui, B. Vickrey, "Seizure reduction and quality of life improvements in people with epilepsy," *Epilepsia*, vol. 43, no. 5, pp. 535-538, May 2002.
- [17] W. Stacey and B. Litt, "Technology insight: neuroengineering and epilepsy - designing devices for seizure control," *Nature Clinical Practice Neurology*, vol. 4, pp. 190-201, Feb. 2008.
- [18] A. Amar, M. Levy, C. Liu, and M. Apuzzo, "Vagus nerve stimulation," in *Proc. IEEE*, vol. 96, no. 7, pp. 1142-1151, Jul. 2008.
- [19] R. Terry, "Vagus nerve stimulation: a proven therapy for treatment of epilepsy strives to improve efficacy and expand applications," in *Proc. Int. IEEE EMBS Conf.*, 2009, pp. 4631-4634.
- [20] D. Shen and Y. Chu, "A linearized current stimulator for deep brain stimulation," in *Proc. Int. IEEE EMBS Conf.*, 2010, pp. 6485-6488.
- [21] S. Santaniello, G. Fiengo, L. Glielmo, and W. Grill, "Closed-loop control of deep brain stimulation: a simulation study," *IEEE Trans. Neural Systems and Rehabilitation Engineering*, vol. 19, no. 1, pp. 15-24, Feb. 2011.
- [22] A. Tzallas, M. Tsipouras, and D. Fotiadis, "The use of time-frequency distributions for epileptic seizure detection in EEG recordings," in *Proc. Int. IEEE EMBS Conf.*, 2007, pp. 3-6.
- [23] C. Suarez, E. Fonoff, M. Munoz, and A. Godoi, "Wavelet transform and cross-correlation as tools for seizure prediction," in *Proc. Int. IEEE EMBS Conf.*, 2010, pp. 4020-4023.
- [24] M. Niknazar, S. Mousavi, B. Vahdat, M. Shamsollahi, and M. Sayyah, "A new dissimilarity index of EEG signals for epileptic seizure detection," in *Proc. IEEE Int. Communications, Control and Signal Processing Symp.*, 2010, pp. 1-5.
- [25] V. Srinivasan, C. Eswaran, and N. Sriraam, "Approximate entropy-based epileptic EEG detection using artificial neural networks," *IEEE Trans. Information Technology in Biomedicine*, vol. 11, no. 3, pp. 288-295, May 2007.
- [26] B. Litt, M. D'Alessandro, R. Esteller, J. Echaz, and G. Vachtsevanos, "Translating seizure detection, prediction and brain stimulation into implantable devices for epilepsy," in *Proc. Int. IEEE EMBS Conf.*, 2003, pp. 485-488.
- [27] B. Litt, "Implantable devices for epilepsy: a clinical perspective," in *Proc. IEEE Int. EMBS Conf.*, 2002, pp. 2035-2036.

- [28] C. Young, S. Liang, D. Chang, Y. Liao, F. Shaw, and C. Hsieh, "A portable wireless online closed-loop seizure controller in freely moving rats," *IEEE Trans. Instrumentation and Measurement*, vol. 60, no. 2, pp. 513-521, Feb. 2011.
- [29] C. Merrill, M. Jonsson, L. Minthon, H. Ejnell, H. Silander, K. Blennow, M. Karlsson, A. Nordlund, S. Rolstad, S. Warkentin, E. Ben-Menachem, and M. Sjogren, "Vagus nerve stimulation in patients with Alzheimer's disease: additional follow-up results of a pilot study through 1 year," *J. Clin Psychiatry*, vol. 67, no. 8, pp. 1171-1178, Aug. 2006.
- [30] X. Liu, A. Demosthenous, and N. Donaldson, "An integrated implantable stimulator that is fail-safe without off-chip blocking-capacitors," *IEEE Trans. Biomedical Circuits and Systems*, vol. 2, no. 3, pp. 231-244, Sep. 2008.
- [31] D. McCreery, T. Yuen, W. Agnew, and L. Bullara, "Neural damage from continuous microstimulation in the cochlear nucleus; correlation with stimulus parameters," in *Proc. IEEE Int. EMBS Conf.*, 1992, pp. 1396-1397.
- [32] A. Ray, L. Chan, B. Thomas, and J. Weiland, "Effects of prolonged stimulation at the electrode-retina interface," in *Proc. IEEE Int. EMBS Conf.*, 2006, pp. 1285-1287.
- [33] M. Ghovanloo and K. Najafi, "A small size large voltage compliance programmable current source for biomedical implantable microstimulators," in *Proc. IEEE Int. EMBS Conf.*, 2003, pp. 1979-1982.
- [34] M. Ghovanloo and K. Najafi, "A compact large voltage-compliance high output-impedance programmable current source for implantable microstimulators," *IEEE Trans. Biomedical Engineering*, vol. 52, no. 1, pp. 97-105, Jan. 2005.
- [35] M. Sivaprakasam, W. Liu, G. Wang, J. Weiland, and M. Humayun, "Architecture tradeoffs in high-density microstimulators for retinal prosthesis," *IEEE Trans. Circuits and Systems I: Regular Papers*, vol. 52, no. 12, pp. 2629-2641, Dec. 2005.
- [36] M.-D. Ker and S.-L. Chen, "Mixed-voltage I/O buffer with dynamic gate-bias circuit to achieve $3xV_{DD}$ input tolerance by using $1xV_{DD}$ devices and single VDD power supply," in *IEEE Int. Solid-State Circuits Conf. Dig. Tech. Papers*, 2005, pp. 524-525.
- [37] M.-D. Ker and Y.-L. Liu, "Design of $2xV_{DD}$ -tolerant I/O buffer with $1xV_{DD}$ CMOS devices," in *Proc. IEEE Custom Integrated Circuits Conf.*, 2008, pp. 539-542.
- [38] V. Prodanov and V. Boccuzzi, "7V tristate-capable output buffer implemented in standard 2.5V CMOS process," in *Proc. IEEE Custom Integrated Circuits Conf.*, 2001, pp. 497-500.
- [39] B. Serneels T. Piessens, M. Steyaert, and W. Dehaene, "A high-voltage output driver in a 2.5-V 0.25- μm CMOS technology," *IEEE J. Solid-State Circuits*, vol. 40,

no. 3, pp. 576-583, Mar. 2005.

- [40] E. Lee, "High-voltage tolerant stimulation monitoring circuit in conventional CMOS process," in *Proc. IEEE Custom Integrated Circuits Conf.*, 2009, pp. 93-96.
- [41] M.-D. Ker, S.-L. Chen, and C.-S. Tsai, "Design of charge pump circuit with consideration of gate-oxide reliability in low-voltage CMOS processes," *IEEE J. Solid-State Circuits*, vol. 41, no. 5, pp. 1100-1107, May 2006.



Vita

姓 名：李 易 儒

學 歷：

私立明道高級中學 (91年9月~94年6月)

國立交通大學電子工程學系 (94年9月~98年6月)

國立交通大學電子研究所碩士班 (98年9月~100年7月)

研究所修習課程：

類比積體電路	吳介琮 教授
數位積體電路	黃 威 教授
積體電路之靜電放電防護設計特論	柯明道 教授
類比濾波器設計	蔡嘉明 教授
半導體物理及元件(一)	汪大暉 教授
計算機結構	劉志尉 教授
數位通訊	林大衛 教授
電力電子導論	鄒應嶼 教授

永久地址：台中市霧峰區五福路 817 號

Email：m9811659@alab.ee.nctu.edu.tw